Applied and
Computational
Mathematics
Division

NISTIR 5641

Computing and Applied Mathematics Laboratory

Anisotropy of Interfaces in an Ordered Alloy: A Multiple-Order-Parameter Model

R. J. Braun, J. W. Cahn, G. B. McFadden, and A. A. Wheeler

April 1995

U.S. DEPARTMENT OF COMMERCE
Technology Administration
National Institute of Standards and Technology
Gaithersburg, MD 20899

NISTIR 5641

Anisotropy of Interfaces in an Ordered Alloy: A Multiple-Order-Parameter Model

R. J. Braun
J. W. Cahn
G. B. McFadden
A. A. Wheeler

U.S. DEPARTMENT OF COMMERCE
Technology Administration
National Institute of Standards
and Technology
Applied and Computational Mathematics Division
Computing and Applied Mathematics Laboratory
Gaithersburg, MD 20899

April 1995

U.S. DEPARTMENT OF COMMERCE
Ronald H. Brown, Secretary

TECHNOLOGY ADMINISTRATION
Mary L. Good, Under Secretary for Technology

NATIONAL INSTITUTE OF STANDARDS
AND TECHNOLOGY
Arati Prabhakar, Director

Anisotropy of Interfaces in an Ordered Alloy: A Multiple-Order-Parameter Model

R. J. Braun*, J. W. Cahn, G. B. McFadden, and A. A. Wheeler†

National Institute of Standards and Technology

Gaithersburg, MD 20899

USA

Abstract

A multiple-order-parameter theory of ordering on a binary face-centered-cubic (FCC) crystal lattice is developed, and adapted to provide a continuum formulation that incorporates the underlying symmetries of the FCC crystal in both the bulk and gradient-energy terms of the free energy. The theory is used to compute the orientation dependence of the structure and energy of interphase and antiphase boundaries. The structure of these interfaces compares favorably with previous lattice calculations by Kikuchi and Cahn. Anisotropy is a natural consequence of the lattice calculation and the multiple-order-parameter continuum formulation presented here. This is in contrast to the *ad hoc* fashion in which anisotropy is often introduced into a single-order-parameter continuum theory.

*Permanent address: Department of Mathematical Sciences, University of Delaware, Newark, DE 19716, USA

†Permanent address: Faculty of Mathematical Studies, University of Southampton, Highfield, Southampton SO17 1BJ, UK.

1. Introduction

In many continuum theories of phase change, such as spinodal decomposition and ordering reactions, the interface between the two phases is regarded as being diffuse rather than sharp, with a finite thickness over which properties vary smoothly from one set of bulk values to another. Such diffuse interface theories arise naturally in the equilibrium descriptions of critical phenomena (Stanley 1971), where the interface thickness scales with the correlation length and diverges as the critical temperature is approached. Recently this approach has been extended to other phase changes, such as solidification, with significant computational advantages for describing such complex behavior as dendritic growth.

Crystalline anisotropy is an important component of many of these phase changes. There have been a variety of methods for introducing the anisotropy into the theory. Some of these arise from physical principles, while others are *ad hoc* and can be the origin of inconsistencies. Some types of anisotropy are associated with the interfaces, while others, such as anisotropic elastic effects, are associated with the volumes, even when they arise from coherency constraints at interfaces (Cahn 1961).

One method for treating diffuse interfaces is to use a free energy functional for the system in terms of continuum parameters that are spatially varying. The functional is written as the integral of the sum of two kinds of terms; bulk energies that are multiple well functions of these parameters that have minima, or common tangents, at values that characterize the adjacent phases, and gradient energies that are functions, commonly the square, of the gradients of the order parameters. Both terms contribute to the energy in the transition regions that separate bulk phases. Such gradient energy models date back to work by Rayleigh (1892) and Van der Waals (1893), and are useful in a variety of contexts.

One such use is for dynamical calculations in which evolution equations for the system are derived by using variational arguments on these free energy functionals. When there is a single nonconserved scalar order parameter, the usual form of the resulting equation is the Cahn-Allen equation (Cahn and Allen 1977; Allen and Cahn 1979) describing antiphase boundary motion between domains of an ordered phase, as described in more detail below. For a single conserved parameter, such as the composition, the result is the Cahn-Hilliard equation (Cahn 1961 and Hilliard 1970) used to describe the spinodal decomposition of a binary alloy. Phase-field descriptions of the

solidification of binary alloys have been developed recently by Wheeler *et al.* (1992,1993a), Caginalp and Xie (1993), and Warren and Boettinger (1995); they can be viewed as combining elements of the Cahn-Allen model and the Cahn-Hilliard model. In many cases gradient energy models can be viewed as mean field approximations to models that provide atomic-level descriptions; examples of such mean field theories are given by the Landau theory of a second-order phase transition (Landau 1937) or density functional theories (see, e.g., Evans 1979 or Oxtoby 1991).

Phase-field models can be particularly useful for numerical computation in situations in which the interphase boundary is expected to be geometrically complicated. For example, during the dendritic growth of a pure material into its undercooled melt, the generation and propagation of sidebranches along the primary branch of the dendrite leads to a wide range of length and time scales, and phase-field models have been employed to provide numerical tests of theories of tip selection (Kessler *et al.* 1988, Glicksman and Marsh 1993, Wheeler *et al.* 1993b). During dendritic growth an important role is played by the crystalline anisotropy of the growing solid phase, which selects the growth direction of the dendrite, the symmetry of the sidebranch structure, and the velocity of the dendrite tip.

For a scalar order parameter, formulations that use the square of a gradient are inherently isotropic. For a phase-field model to be of practical importance, it must include a description of the anisotropic nature of the crystal, through such effects as the dependence of the solid-liquid surface free energy (sometimes called the surface tension) on the interface orientation with respect to the crystal lattice, and also the variation of the rate of attachment kinetics with interface orientation. One way that anisotropic effects have been modeled is to allow the phenomenological phase-field parameters (such as the gradient energy coefficient and the mobility coefficient for temporal relaxation) to depend on the direction of the gradient of the phase field parameter (Kobayashi 1993). It is possible to re-express the gradient energy term as the square of a function of the gradient which is homogeneous of degree one (Taylor and Cahn 1994); these two forms for the anisotropy are equivalent. This approach is an example where the anisotropy is introduced in an *ad hoc* manner, and its connection with the underlying crystalline anisotropy is indirect. Still, it successfully generalizes the original isotropic phase-field methodology to allow the computation of dendrites with the proper qualitative behavior, and leads to the proper anisotropic version of the Gibbs-Thompson equation at the crystal-melt interface in the sharp interface limit (McFadden *et*

al. 1993, Wheeler and McFadden 1995). With this type of formulation, anisotropies with general symmetries can be treated using a single order parameter; for example, two-dimensional dendrites with six-fold symmetry can be computed using finite differences on a rectangular mesh (Murray *et al.* 1994; Warren and Boettinger 1995).

Anisotropy occurs naturally in discrete lattice calculations of interfaces (see, e.g., Herring 1951, Frank 1962). The symmetry of a crystal imposes symmetry constraints on the properties of both bulk and interfacial properties. For example, it is well known that for bulk diffusion processes the second rank conductivity tensor is constrained to be isotropic for a cubic material. In contrast, surface energies are generally not tensor properties, and even cubic crystals are expected to have anisotropic interfacial properties. The symmetry constraints for surfaces between two crystalline phases depends on both their symmetries and their relative positioning.

Anisotropy that is inherent in a lattice description can be lost when lattice models are approximated by continuum descriptions that employ gradient energy terms. For a single order parameter (Cahn and Hilliard 1958), gradient energy coefficients become matrices or second rank tensors. For cubic crystals this results in an isotropic tensor, and the gradient energy reduces to the square of the gradient, leading to an isotropic surface energy. For crystals of lower symmetry a quadratic gradient energy term can be made isotropic by a rescaling of the spatial coordinates, and so the computed anisotropy in the physical system is restricted to a simple (elliptical) form.

Ordering reactions in crystalline solids provide a number of simple types of interfaces with anisotropies that are constrained by symmetry arguments. We distinguish two general types: interphase boundaries (IPBs) between two different ordered phases or between an ordered and a disordered phase, and antiphase boundaries (APBs) between two domains of ordered variants of the same phase. The elucidation of the symmetry properties in terms of Shubnikov groups is particularly simple, if the inversion centers of both abutting phases fall on a common lattice (Kalonji and Cahn 1982). In that case the dependence of the interface properties on the direction of the interface normal are constrained by the intersection group of the two abutting domains.

Since the ordering reaction generally produces a phase with symmetry properties that form a subgroup of those of the disordered phase, the symmetry properties for the IPB are those of the ordered phase. For the APB, the symmetry depends on the relative positioning of the two domains; symmetries that are no longer common to both domains are lost. For particular orderings in two

cubic lattices, bcc and fcc, to give cubic ordered phases, general symmetry arguments (Kikuchi and Cahn 1962, 1979) show that the APB between two cubic ordering domains has cubic symmetry for ordering to the $B2$ and $DO3$ structures in bcc and tetragonal symmetry for ordering to the $L1_2$ structure in fcc. (The prototypes for these structures are respectively, CsCl (or β brass), BiF_3 (or Fe_3Al) and Cu_3Au.) Thus the different orderings studied in these two cubic lattices illustrate another distinct source of the interfacial anisotropy in lattice models.

Kikuchi and Cahn have performed discrete calculations for both bcc (Kikuchi and Cahn 1962) and fcc lattices (Kikuchi and Cahn 1979) for a limited set of orientations as a function of temperature and composition. In the case of bcc, the lattice calculations were compared with isotropic continuum calculations.

In this paper we examine interfacial anisotropy between parallel cubic phases or domains using a continuum formulation with multiple order parameters that preserves the underlying anisotropies of the crystalline lattice. We will focus on binary alloy fcc crystals in the context of the order-disorder transition that give the tetragonal symmetry. We derive the continuum gradient energy model and use it to obtain for all orientations the orientation dependence of the structure and free energy of static planar antiphase and interphase boundaries. We compare the results obtained with those obtained for a limited set of orientations by Cahn and Kikuchi (1985) using cluster variation methods and by Landman *et al.* (1980,1981) and Cleveland *et al.* (1982) using molecular dynamics simulations of solidification. We note the facetting and wetting transitions in these interfaces. Interfacial energies can be used to compute equilibrium microstructural shapes, such as single particles in a matrix (the Wulff shapes) and domain structures, which for Cu_3Au have long been known to show a high degree of anisotropy (Fisher and Marcinkowski 1961). We will ignore elastic effects due to mismatching lattice parameters between the phases. These are important only for the coherent coexistence of large-enough particles of a phase with a different lattice parameter in a matrix or in domain structures of noncubic phases. Depending on the mismatch parameter, the size where elastic effects become important can be as small as nanometers.

2. Formulation

In this section, we discuss bcc and fcc ordering in discrete and continuum formulations. We begin with a brief description of the crystallography of ordering interfaces (Section 2.1), followed by a

discussion of the formulation of discrete models and issues in taking such models to continuum limits (Section 2.2). We then discuss a specific simple continuum model of ordering on a bcc lattice (Section 2.3), in order to motivate the more general continuum model which we shall study in this paper (Section 2.4).

2.1. Ordering interface crystallographies

Ordering in a bcc crystal produces a phase with the CsCl structure (designated as B2, with space group symmetry *Pmmm*), in which the two primitive cubic sublattices are occupied with different atoms and hence are not equivalent (see Figure 1). The transition is higher order with the usual

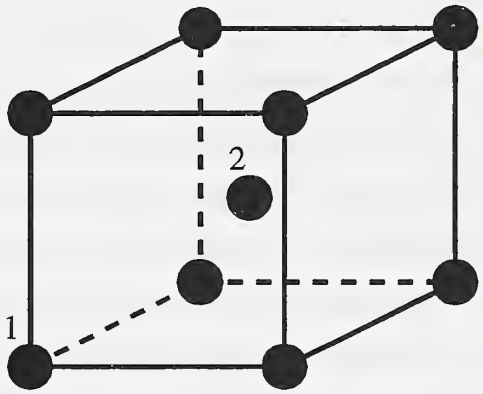

Figure 1: A schematic diagram of the unit cell of a bcc lattice. The sites 1 and 2 are distinguished.

statistical mechanical models, although it can be first order. When the transition is higher order there is no coexistence between the ordered and disordered phase and no interfaces between these two phases. The ordering is a subgrouping of order 2 and produces two domains that are shifted relative to one another by a vector, $(1/2) < 111 >$, which had been a translation vector in bcc, but is no longer a translation vector in the ordered cubic phase.

The special point symmetry of this shift vector is compatible with cubic symmetry for the APB, however. One way to see this is that all shift vectors of type $(1/2) < n_1, n_2, n_3 >$, where the n_i are odd integers, are equivalent to $(1/2) < 111 >$ by addition of lattice translations of the periodic ordered lattice; therefore all translations of type $(1/2) < \pm 1 \pm 1 \pm 1 >$, describe the same APB. Such an equivalence means that such a shift does not distinguish among axes, and does not break

the equivalence of the three cubic axes. This leads to a cubic ($m3m$) symmetry for the properties of the APB that depend on the direction of its normal. This can also be seen by noting that three and four-fold axes of one domain continue in the other. Near the order-disorder transition the APB interface thickness diverges and is large compared to the lattice parameter. As a result, the isotropic continuum approximation is found to become valid (Cahn and Kikuchi 1962) and leads to isotropic interfaces. Anisotropy corresponding to the $m3m$ cubic symmetry is found at lower temperatures.

By contrast, the ordering of fcc to the $L1_2$ structure (with space group $Pm3m$; prototype Cu_3Au) gives four interpenetrating primitive cubic lattices, as seen in Figure 2. This ordering

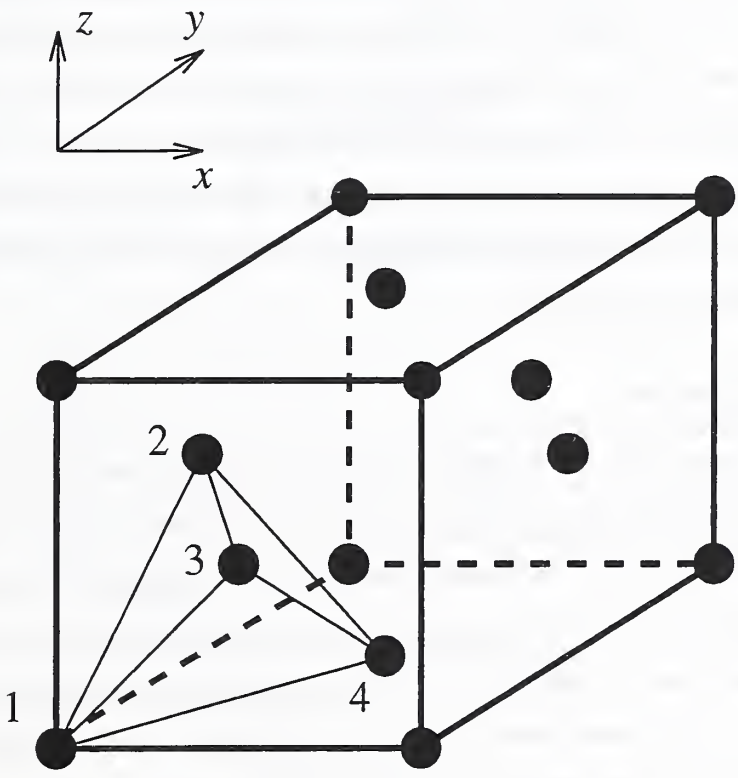

Figure 2: A schematic diagram of an fcc lattice. There are four distinguished sites corresponding to a corner and one each for the faces intersecting at that corner.

transition cannot be a higher-order transition (Landau and Lifshitz 1980). At the transition temperature there is coexistence between the ordered and disordered cubic phase and hence there is an IPB between them. The symmetry of the orientational properties of the IPB is also $m3m$;

there is no reason for to it be isotropic. APBs are interfaces between any two of the four ordered domains that are shifted by a vector of type $(1/2) < 110 >$ relative to one another. Such shifts between two cubic domains break the symmetries among the three cube axes; although the axes of the two domains are parallel, all are shifted, and two of them cease to be four-fold axes of the two-domain system. In one cube direction a four-fold axis through the cube corners in one domain is retained, and continues as a four-fold axis through the face center in the other domain. The four-fold axes of the other two cube directions continue as two-fold axes in the other domain, and are lost as four-fold axes. The shift also means that no three-fold axis threads both domains. This leads to interfaces with a lowered tetragonal symmetry ($4/mmm$) in their orientational properties. The anisotropy due to this tetragonality was found to be severe enough to make some orientations unstable (Kikuchi and Cahn 1979); the interfacial energy is a nonconvex function of orientation. Furthermore there are structural changes in the interface with increasing temperature, that are described as an infinite set of interfacial phase transitions (Finel *et al.* 1990). A proper continuum model should preserve the tetragonal anisotropy due to the $(1/2)< 110 >$ shift. The continuum model developed in this paper will give the tetragonal symmetry for the APB and at the same time will yield cubic anisotropy in the IPB.

2.2. Discrete formulations

In a binary alloy with no vacancies there would appear to be only one composition variable. The alternation in composition between neighboring sites that describes a known ordered structure can lead to the formulation of ill-posed differential equations if they are couched in a spatially continuous composition variable. This problem can be avoided by a formulation with suitable choices of a number of order parameters in addition to the local composition, even though it creates a set of field variables from a single composition. A study of spatially discrete formulations for bcc and what happens when the spatial variable is continuized was recently done, and set guidelines for how the order parameter should be chosen (Cahn and Novick-Cohen 1994).

In a discrete formulation, the assumptions of pairwise interactions in a binary alloy of A and B atoms implies that there are energy terms in the free energy of the form

$$\sum_{\mathbf{i}} \sum_{\mathbf{j}} \alpha_{\mathbf{j}} \rho^{(\mathbf{i})} \rho^{(\mathbf{i}+\mathbf{j})},$$

where $\rho^{(\mathbf{k})}$ is the probability that an A atom sits on a lattice site whose position is parametrized by three integers, designated by $\mathbf{k} \in \mathbf{Z^3}$, and and $\alpha_\mathbf{j}$ is the energy associated with finding two A atoms separated by $\mathbf{j}$. The point group symmetry dictates which sets of $\mathbf{j}$ have the same value of α. While it is possible to choose basis vectors such that every element of Z^3 is a lattice point, it is convenient for bcc and fcc to let the basis vectors be along the cube edges. In order to avoid half-integer values in the position vector, we choose 2 as the edge length of the unit cell, and put restrictions on integer values of the components of $\mathbf{k}$. For bcc, the component of $\mathbf{k}$ are then either all even (cube corners) or all odd (body centres); a $< 111 >$ translation of the origin switches corner and centres. For fcc, the sum of the components has to be even; all even components denote cube corners, while two odd components denote face centres.

Let us examine the properties of one such term in the free energy

$$\sum_\mathbf{i} \sum_\mathbf{a} \alpha_\mathbf{a} \rho^{(\mathbf{i})} \rho^{(\mathbf{i+a})},$$

where $\mathbf{a}$ is a vector belonging to the set of vectors $\mathbf{A} =< 111 >$, which give the locations of the nearest neighbors for bcc. This can be rewritten for an infinite lattice

$$\alpha_\mathbf{a} \rho^{(\mathbf{i})} \rho^{(\mathbf{i+a})} = \frac{\alpha_\mathbf{a}}{2} \sum_\mathbf{i} \left[2(\rho^{(\mathbf{i})})^2 - \left(\rho^{(\mathbf{i})} - \rho^{(\mathbf{i+j})} \right)^2 \right].$$

Continuizing the second term leads to the integral of the square of the gradient of the continuous variable ρ, $-(\alpha_j/2) \int |\nabla \rho(\mathbf{r})|^2 \mathbf{dr}$. When $\alpha > 0$, such a term would lead to ill-posed equations for energy minimization; however, $\alpha > 0$ is what leads to ordered structures, and poses no problem in discrete minimizations of the energy.

To understand the differences in formulations in different lattices we arbitrarily take the species A to be the minority species. Since A atoms are conserved

$$\frac{1}{N} \sum_i^N \rho^{(\mathbf{i})} \equiv W \leq 1/2,$$

where W is the average composition and there are N lattice points. When $\alpha_j < 0$, the minimum in the sum $\sum_\mathbf{i} \alpha_\mathbf{j} \rho^{(\mathbf{i})} \rho^{(\mathbf{i+j})}$ tends to occur when A atoms are compactly clustered on sublattices whose basis vector are taken from the set $\mathbf{j}$; when $\alpha_\mathbf{j} > 0$, the minimum in the sum tends to occur when as few pairs as possible are A atoms are separated by the vector $\mathbf{j}$. This is achieved when A and B can alternate along such sublattices. Alternation is not possible on close-packed sublattices, i.e. on

fcc itself with the j chosen from the set of near neighbor $< 110 >$, or on bcc with the set of third neighbor $< 220 >$, because there are closed equilateral triangles with sides j; this leads to what is called frustration.

In what follows, we will call α_1 and α_2 the values of α for first and second neighbors, and we assume that $\alpha = 0$ for all higher neighbors. If $\alpha_1 < 0$, the minimum in the sum $\sum_{\mathbf{i}} \alpha_{\mathbf{j}} \rho^{(\mathbf{i})} \rho^{(\mathbf{i+j})}$ occurs when $\rho_i = 1$ for a compact cluster occupying a fraction $\int \rho(\mathbf{r}) d\mathbf{r} / \int d\mathbf{r}$ of the lattice points and $\rho_i = 0$ for the remaining points. This is a structure on the lattice that can be described as phase separated into pure A and pure B phases. Spinodal decomposition can be modeled with a single negative near neighbor interaction.

Interesting cases occur when α_1 and α_2 are respectively positive and negative. For both fcc and bcc, points linked by second neighbors with its negative α_2 form simple cubic sublattices. The interaction term will be at its minimum when the minority species will concentrate as clusters on no more than half of the sublattices (one for bcc and one or two for fcc). With both interactions for bcc the minimum in energy occurs when ρ_i alternates between 0 and 1 for compact clusters occupying a fraction $2W$ of the lattice points and $\rho_i = 0$ for the remaining points. This is a structure on the lattice that can be described as phase separated into an ordered B2 phase and a pure B phase. When $W = 1/2$ the minimum is for the B2 structure alone. For fcc the situation depends on W. When $W = 1/4$ the minimum is the $L1_2$ structure, and the minority A atoms occupy one of the four primitive cubic sublattices of the fcc. For $0 < W < 1/4$, the minimum is a mixture of an fcc that is pure B and $L1_2$; the A occupy a part of that one sublattice. For $W = 1/2$ the minimum occurs for the $L1_0$ structure (space group symmetry P4/mmm, prototype CuAu) in which two of the sublattices are occupied by A; an equivalent description is a layering on a cube plane, alternating in pure A and pure B. For $1/4 < W < 1/2$ the minimum is for a mixture of $L1_2$ and $L1_0$. The minima occur for two-phase structures with minimum area for the "surface" between the phases (Richards and Cahn 1971).

What emerges from such considerations is that, except for interfaces, the compositions on each sublattice (two for bcc and four for fcc) can be thought of as slowly varying or constant over large distances. Linear combinations of these variable give a new slowly varying composition variable averaged over the sublattices, and even over some larger neighborhood, that is subject to the conservation condition. Other combinations lead to slowly varying order parameters, which need

not be conserved. If the selection of these variable is done properly it leads to well posed equations whose solutions can be shown to approximate those of the discrete equations. The three-order-parameter model considered here describes the ordering of an fcc crystal in much the same way that the Cahn-Allen equation, a model with a single order parameter, describes the ordering of a bcc alloy.

2.3. The bcc alloy

We review briefly the case of a bcc alloy in a way that differs from that used by Cahn and Novick-Cohen (1994); this helps clarify the meaning of the order parameters we will use in the fcc model, and shows in what sense the three-order-parameter model can be viewed as a generalization of the Cahn-Allen equation.

A simple model is obtained by assuming the state of the system can be characterized by just two parameters ρ_1 and ρ_2 giving the atomic fraction of component A at sites 1 (corners) and 2 (body centres), respectively; the atomic fraction of the full system is then $W = (\rho_1 + \rho_2)/2$. The parameters ρ_1 and ρ_2 can be viewed as average values of the atomic fraction of A over each sublattice; a disordered state of the crystal in which A and B atoms are spread randomly over sites 1 and 2 is then described by $\rho_1 = \rho_2 = W$. An ordered state of the crystal is one in which the sites 1 and 2 are differentially populated by A and B atoms, so that $\rho_1 \neq \rho_2$. This simple two-parameter model clearly describes only long range ordering; the description of local arrangements of more than a pair of sites requires the introduction of additional variables as done in the cluster variation method (Kikuchi 1951).

To convert the rapidly alternating composition of the ordered structure into slowly varying composition field, it is convenient either to deal with each sublattice separately or to change variables and work instead with the parameters

$$W = \frac{1}{2}(\rho_1 + \rho_2), \qquad X = \frac{1}{2}(\rho_1 - \rho_2); \tag{1}$$

a disordered state of the crystal is therefore described by $X = 0$, and X is nonzero in an ordered state. Conservation of atomic species is a constraint on the average composition W, but not on the order parameter X, which need not be conserved as the crystal undergoes transitions between ordered and disordered states.

In this model the thermodynamic state of an isothermal crystal is described by a Helmholtz free energy density f that is assumed to depend on the atomic fractions ρ_1 and ρ_2, or equivalently on W and X, viz., $f = f(W, X)$. Bulk equilibrium states of a fixed composition are then obtained by minimizing the free energy subject to the constant W = constant, which gives the conditions

$$f_W(W, X) = \lambda, \qquad f_X(W, X) = 0, \tag{2}$$

where λ is a Lagrange multiplier associated with the composition constraint. Disordered bulk states are described by $f_X(W, 0) = 0$; i.e., the free energy has a minimum in X at $X = 0$. Ordered states have non-zero roots in X to the equation $f_X(W, X) = 0$.

2.3.1. Symmetry requirements on the energy

Since a translation of the origin of the crystal from a corner to a body centre reverses the roles of lattices 1 and 2, the free energy density of the crystal should be invariant to the interchange of ρ_1 and ρ_2, or, in terms of W and X, $f(W, X)$ should be an even function of X. If (W, X) represents an ordered equilibrium state with $X \neq 0$, then the solution $(W, -X)$ represents the same physical state, but shifted from the original by a $(1/2) < 111 >$ translation along the cube diagonal.

In order to describe spatially-inhomogeneous crystals with a continuum formulation, it is convenient to allow the parameters X and W to vary slowly in space compared to the lattice spacing. If X is the only spatial variable, Cahn and Allen (1977) postulated a generalized free energy functional of the form

$$\mathcal{F}[W, X] = \int_V \left[\frac{\epsilon^2}{2} |\nabla X|^2 + f(W, X) \right] dV, \tag{3}$$

where the gradient energy coefficient ϵ can be related to the characteristic thickness of transition regions between bulk phases. The gradient energy term provides an energy penalty for sharp transition regions where the gradient of the order parameter is large. In the spirit of the Cahn-Hilliard treatment for a conserved order parameter, a gradient energy contribution involving $|\nabla W|^2$ might also be considered, but we will not treat this possibility since our intent is not to emphasize the isotropic role played by W in the present development.

Dynamical equations for the free energy function (3) can be postulated based on variational arguments, leading to equations of the type

$$\frac{\partial W}{\partial t} = M_W \nabla^2 \frac{\delta \mathcal{F}}{\delta W}, \qquad \frac{\partial X}{\partial t} = -M_X \frac{\delta \mathcal{F}}{\delta X}, \tag{4}$$

where M_W and M_X are phenomenological rate constants relating the time derivatives to the variational derivatives of $\mathcal{F}$. With an appropriate choice of boundary conditions, these equations ensure that W is conserved in time, whereas the order parameter X simply evolves in the direction of steepest descent of $\mathcal{F}$. This will be discussed further in a subsequent paper.

In many instances the time scales associated with ordering on the atomic scale are much faster than those associated with long-range diffusion of the conserved species, so that the kinetics of the non-conserved order parameter are much faster than those associated with the conserved one. Under these conditions it is of interest to consider the evolution of the non-conserved order parameter while assuming that W is uniform in space and time. The equations then reduce to the Cahn-Allen equation

$$\frac{1}{M_X}\frac{\partial X}{\partial t} = \epsilon^2 \nabla^2 X - \frac{\partial f}{\partial X}. \tag{5}$$

A particularly tractable model is obtained by assuming that $f(X)$ has the form of a quartic polynomial with double-well structure of the form

$$f(X) = \frac{f_0}{8}\left[1 - \left(\frac{X}{X_0}\right)^2\right]^2, \tag{6}$$

where $f_0/8$ is the height of the double well at $X = 0$; the energy at the minimum of the double well at $X = X_0$ has been set to zero. The equation then admits a steady state one-dimensional solution of the form

$$X(\zeta) = X_0 \tanh\left(\frac{\zeta}{2X_0\epsilon/\sqrt{f_0}}\right) \tag{7}$$

representing an antiphase boundary (APB) separating two ordered bulk regions with $X = \pm X_0$ by an interfacial region of width $X_0\epsilon/\sqrt{f_0}$. The surface energy γ associated with the APB is given by the excess free energy per unit area of the layer,

$$\gamma = \int_{-\infty}^{\infty}\left[\frac{\epsilon^2}{2}\left(\frac{dX}{d\zeta}\right)^2 + f(X)\right] d\zeta = \frac{2}{3}X_0\epsilon\sqrt{f_0}. \tag{8}$$

2.4. The fcc alloy

We next consider a model for order-disorder transitions on an fcc crystal lattice described geometrically by four inter-penetrating cubic sublattices defined by the lattice points labeled 1, 2, 3, and 4, respectively (see Fig. 2). For the disordered fcc structure all sublattices are crystallographically equivalent. In the Figure 2, the site 1 is chosen to be the corner of the fcc cube, sites 2, 3 and 4

correspond to the face centres of the planes $x = 0$, $y = 0$, and $z = 0$, respectively. The overall state of the crystal is then assumed to be completely described by the four parameters ρ_1, ρ_2, ρ_3, and ρ_4 representing the atomic fraction of A on each sublattice.

It is convenient to introduce four new parameters W, X, Y, and Z in place of the parameters ρ_1, ρ_2, ρ_3, and ρ_4; they are defined by

$$W = \frac{1}{4}(\rho_1 + \rho_2 + \rho_3 + \rho_4), \tag{9a}$$

$$X = \frac{1}{4}(\rho_1 + \rho_2 - \rho_3 - \rho_4), \tag{9b}$$

$$Y = \frac{1}{4}(\rho_1 - \rho_2 + \rho_3 - \rho_4), \tag{9c}$$

$$Z = \frac{1}{4}(\rho_1 - \rho_2 - \rho_3 + \rho_4). \tag{9d}$$

As in the bcc model given above, the parameter W represents the atomic fraction of the system as a whole, and X, Y, and Z are non-conserved order parameters that can vary between plus and minus one half. In this model a disordered state is represented by $\rho_1 = \rho_2 = \rho_3 = \rho_4 = W$, which implies that $X = Y = Z = 0$. The above expressions can be inverted to give the ρ_i as functions of the W, X, Y and Z.

We next consider a thermodynamic description of the crystal for the case of an isothermal system, based on a generalized free energy functional assumed to have the form

$$\mathcal{F} = \int_V \left\{ f(W, X_1, X_2, X_3) + a_{jk} \frac{\partial W}{\partial x_j} \frac{\partial W}{\partial x_k} + b_{jlkm} \frac{\partial X_j}{\partial x_l} \frac{\partial X_k}{\partial x_m} \right\} dV. \tag{10}$$

For notational convenience we have suppressed the dependence of the free energy on temperature, and the suffix notation is given by $X_1 = X$, $X_2 = Y$, $X_3 = Z$, and $(x_1, x_2, x_3) = (x, y, z)$; repeated indices are summed. The term $f(W, X_1, X_2, X_3)$ is the bulk Helmholtz free energy density, and the remaining terms are gradient energy contributions.

As discussed in the next section, the symmetries associated with the fcc crystal structure restrict the possible forms of f, a_{jk}, and b_{jlkm}. In the following section, we will discard the a_{ij} term, since symmetry considerations require that these terms lead only to isotropic contributions. We will also take f to be a low order polynomial in X_1, X_2, X_3, and will assume that the coefficients b_{jlkm} are independent of W.

2.4.1. Symmetry requirements for bulk free energy density

A free energy $f(W, X, Y, Z)$ must have the symmetries in the variables X, Y, and Z that are dictated by the fcc lattice. A rotation of the crystal about the three-fold axis along the cube diagonal through lattice site a effectively re-labels the lattice sites according to the scheme

$$1 \to 1,\ 2 \to 3,\ 3 \to 4,\ 4 \to 2. \tag{11}$$

Using Eq. (9), it follows that permuting ρ_2, ρ_3, and ρ_4 gives rise to the permutation

$$X \to Y,\ Y \to Z,\ Z \to X. \tag{12}$$

It follows that the function $f(W, X, Y, Z)$ must be invariant to cyclic permutations of the three variables X, Y, and Z.

Another symmetry is obtained if the crystal is rotated by π about an axis that passes through the midpoints of the two line segments that join sites 1 and 4 and sites 2 and 3; this rotation interchanges sites 1 and 4 and sites 2 and 3. Using Eq. (9), it follows that under this permutation one has

$$X \to -X,\ Y \to -Y,\ Z \to Z. \tag{13}$$

The function $f(W, X, Y, Z)$ must therefore be invariant to changes in the signs of any two of the variables X, Y, and Z.

In what follows we restrict our attention to a free energy density $f(W, X, Y, Z)$ that is given by a low-degree polynomial. Imposing the above symmetries implies that the energy can be written in the form

$$\begin{aligned} f(W,X,Y,Z) = {} & a_0 + a_2(X^2+Y^2+Z^2) + a_3XYZ + a_{41}(X^4+Y^4+Z^4) \\ & + a_{42}(X^2Y^2+X^2Z^2+Y^2Z^2) + a_5XYZ(X^2+Y^2+Z^2) + a_{61}(X^6+Y^6+Z^6) \\ & + a_{62}\left\{X^4(Y^2+Z^2)+Y^4(X^2+Z^2)+Z^4(X^2+Y^2)\right\} + a_{63}X^2Y^2Z^2 \end{aligned} \tag{14}$$

through terms of degree six, where the coefficients are generally functions of W (and temperature). We note that symmetry permits the cubic term XYZ in the free energy, which plays a fundamental role in the subsequent analysis. The order parameters do not transform in the manner of the components of a vector under simple rotations; for example, a rotation of the crystal by $\pi/4$ about

the z axis effectively interchanges the roles of ρ_2 and ρ_3 while leaving ρ_1 and ρ_4 unchanged. This implies that X and Y are interchanged with no change in sign, whereas such a rotation would be expected to produce a sign change in one of the components of a vector quantity.

A free energy of this type can provide correct qualitative descriptions of the disordered fcc phase (vanishing order parameters) and two of the commonly-observed ordered phases that occur in fcc systems (Ansara *et al.* 1988, Dupin 1995). In a temperature-composition phase diagram, the $L1_0$ ordered phase has a congruent temperature located at or near the composition $W = 1/2$; this phase is described by a single non-zero order parameter. The $L1_2$ ordered phases have congruent temperatures located at compositions at or near $W = 1/4$ (for the stoichiometry A_3B) and $W = 3/4$ (for AB_3); for the $L1_2$ phase all three order parameters are non-zero and are equal in absolute value. A phase diagram with the correct qualitative features can be obtained with this free energy by prescribing an appropriate temperature and composition dependence to the coefficients a_0, a_2, and a_3; the higher-degree coefficients may be taken to be constants. The fcc-$L1_0$ phase transition is first order if a_{41} and a_{61} are negative and positive, respectively, and the fcc-$L1_2$ transition is first order if the coefficient a_3 is non-zero (Braun *et al.* 1995b). More generally, one would choose the coefficients in the free energy to obtain agreement with a given phase diagram or other measured properties of the alloy, such as heat capacity or equilibrium pair correlations (Clapp and Moss 1966, 1968; Moss and Clapp 1968), or first principle quantum mechanical calculations (de Fontaine 1994).

In the work described herein, we will focus on the fcc-$L1_2$ phase transition, and will simplify the analysis by truncating the free energy at fourth degree and assuming that the fourth-degree terms are positive definite. Such a truncation would not provide a correct description of the fcc-$L1_0$ transition at $W = 1/2$; instead, one obtains the multicritical point of second-order transitions originally found by Nix and Shockley (1938). In future work we plan to investigate the sixth-degree theory; however, we may note that it is possible to choose the free energy coefficients in the sixth-degree theory in such a way that the fcc-$L1_0$ transition remains first order, while in the expression for the bulk energy of the $L1_2$ phase the fifth and sixth degree terms are absent. Preliminary studies indicate that the results obtained here for the fcc-$L1_2$ transition are in qualitative agreement with a more realistic sixth-degree model. In the present work we will describe phase boundaries by prescribing the coefficients a_2, a_3, a_{41} and a_{42} themselves; without loss of generality we will set $a_0 = 0$. Since our principal concern is with the surface tension anisotropy introduced by the multiple

order parameters, we will also simplify the model by ultimately assuming that the composition W is uniform throughout the system. Except at a congruent point, the equilibrium compositions for a two-phase system would be expected to differ; assuming a uniform composition generally is equivalent to working along T_0 curves in the phase diagram that describe states of equal free energies (see, e.g., Cahn 1971 for a discussion of T_0 curves).

2.4.2. Symmetry requirements for the gradient energies

The form of the two terms in the gradient energy contribution, denoted by $S(\mathrm{x})$, is

$$S(\mathrm{x}) = a_{jk}\frac{\partial W}{\partial x_j}\frac{\partial W}{\partial x_k} + b_{jlkm}\frac{\partial X_j}{\partial x_l}\frac{\partial X_k}{\partial x_m}. \tag{15}$$

We require that $S(\mathrm{x})$ transform like a scalar under simple rotations of the crystal. Since W is a scalar, we find that the coefficients a_{jk} form an isotropic second rank tensor. However, the b_{jlkm} do not transform in the manner of a fourth-rank tensor, since as noted above the X_j do not form a first-rank tensor. The partial derivatives $\partial X_j/\partial x_l$ themselves do not constitute a second-rank tensor, and hence the coefficients b_{jlkm} obey a different transformation law in order that $S(\mathrm{x})$ results in a scalar quantity.

If the nine derivatives $\partial X_j/\partial x_l$ are arranged in a 9×1 linear array, then the coefficients b_{jklm} can be arranged in a corresponding 9×9 array having 81 elements. Since S is then given by a quadratic form based on this array, the array may be chosen to be a symmetric matrix with $b_{jlkm} = b_{kmjl}$, and the number of independent coefficients is reduced to 45. By invoking the symmetry of the fcc crystal, the number of independent coefficients reduces to two, and $S(\mathrm{x})$ can be written in the simple form

$$b_{jlkm}\frac{\partial X_j}{\partial x_l}\frac{\partial X_k}{\partial x_m} = \frac{A}{2}\left(X_x^2 + Y_y^2 + Z_z^2\right) + \frac{B}{2}\left(X_y^2 + X_z^2 + Y_x^2 + Y_z^2 + Z_x^2 + Z_y^2\right). \tag{16}$$

where A and B are independent constants. To give an example of the arguments that are involved, consider a set of order parameters with $X = g_0(x)$ and $Y = Z = 0$, which results in the expression

$$S(\mathrm{x}) = b_{1111}\, g_0'(x)\, g_0'(x). \tag{17}$$

Now consider a four-fold rotation of the crystal about the z-axis, so that $x \to y$ and $y \to -x$; that is, the coordinates of a point $\mathrm{x} = (x_0, y_0, z_0)$ fixed in the crystal are now $\mathrm{x}' = (-y_0, x_0, z_0)$ (here

we regard the coordinate system as fixed and rotate the crystal). Under the rotation, the densities change according to

$$\rho_1 \rightarrow \rho_1,\ \rho_2 \rightarrow \rho_3,\ \rho_3 \rightarrow \rho_2,\ \rho_4 \rightarrow \rho_4. \tag{18}$$

In addition, since the crystal is assumed to have property variations along the coordinate x in the original orientation, after rotation the properties of the crystal now vary along the y direction of the fixed coordinate system. Thus, the order parameters as measured in the fixed coordinate system that are associated with the new orientation of the rotated crystal are given by

$$X = 0,\ Y = g_0(y),\ Z = 0. \tag{19}$$

The quantity S that is computed for the rotated crystal is then

$$S(\mathrm{x}') = b_{2222}\, g_0'(y)\, g_0'(y). \tag{20}$$

If we require that the computation of S gives the same result for corresponding points in the original and new orientations of the crystal, we then conclude that $b_{1111} = b_{2222}$. By invoking similar arguments, it can be shown that the gradient energy contribution has the above form.

An alternate, heuristic motivation of the form of the gradient energy term can be based on near-neighbor interactions on the fcc lattice. To do this, a lattice parameter d is introduced that represents the length of the unit cell, and we introduce the notation

$$\rho_1^{(j,k,l)} = \rho_1(jd, kd, ld), \tag{21}$$

for the representation of the atomic fraction of sublattice 1 at the points $x = jd$, $y = kd$, and $z = ld$, and analogous definitions for the other sublattices,

$$\rho_2^{(j,k+1/2,l+1/2)} = \rho_2(jd, [k+1/2]d, [l+1/2]d), \tag{22}$$

$$\rho_3^{(j+1/2,k,l+1/2)} = \rho_3([j+1/2]d, kd, [l+1/2]d), \tag{23}$$

$$\rho_4^{(j+1/2,k+1/2,l)} = \rho_4([j+1/2]d, [k+1/2]d, ld). \tag{24}$$

The discrete free energy is assumed to consist of contributions from pointwise energies and from nearest- and second nearest-neighbor interactions.

The second-nearest-neighbor interactions involve points on the same cubic sublattices; a representative interaction has the form $-\beta\, \rho_1^{(j+1/2,k,l)}\, \rho_1^{(j,k,l)}$, which can be re-expressed in the form of

simple finite differences plus pointwise contributions as in Section 2.2. In the continuum limit the second nearest-neighbor interactions then contribute the gradient term

$$\mathcal{F}^{(2)} = \frac{\tilde{B}}{8} \int_V \left(|\nabla \rho_1|^2 + |\nabla \rho_2|^2 + |\nabla \rho_3|^2 + |\nabla \rho_4|^2 \right\} \, dV, \tag{25}$$

where $\tilde{B}$ is proportional to the second nearest-neighbor interaction energy β. Inserting the definitions of the atomic fractions in terms of the order parameters gives

$$\mathcal{F}^{(2)} = \frac{\tilde{B}}{2} \int_V \left\{ |\nabla X|^2 + |\nabla Y|^2 + |\nabla Z|^2 \right\} \, dV. \tag{26}$$

The nearest-neighbor interactions are less straightforward, since they involve coupling between sublattices. A typical interaction is a product of the form $\alpha \, \rho_1^{(j,k,l)} \, \rho_3^{(j+1/2,k,l+1/2)}$, and the sum of the four terms involving the interaction of $\rho_1^{(j,k,l)}$ with sublattice 3 contributes an expression of the form

$$\begin{aligned} &\alpha \rho_1^{(j,k,l)} \left\{ \rho_3^{(j+1/2,k,l+1/2)} + \rho_3^{(j+1/2,k,l-1/2)} + \rho_3^{(j-1/2,k,l+1/2)} + \rho_3^{(j-1/2,k,l-1/2)} \right\} \\ &\qquad \approx \frac{\alpha d^2}{2} \rho_1 \left\{ \frac{\partial^2 \rho_3}{\partial x^2} + \frac{\partial^2 \rho_3}{\partial z^2} \right\} + \text{bulk contributions} \end{aligned} \tag{27}$$

to the gradient energy expression in the continuum limit. Collecting all the terms that involve x-derivatives gives the contribution

$$\begin{aligned} \mathcal{F}_x^{(1)} &= \frac{\tilde{A}}{4} \int_V \left[(\rho_1 + \rho_2) \frac{\partial^2}{\partial x^2} (\rho_3 + \rho_4) + (\rho_3 + \rho_4) \frac{\partial^2}{\partial x^2} (\rho_1 + \rho_2) \right] \, dV \\ &= -\frac{\tilde{A}}{2} \int_V \left[(\rho_1 + \rho_2)_x (\rho_3 + \rho_4)_x \right] \, dV = \frac{\tilde{A}}{2} \int_V X_x^2 \, dV, \end{aligned} \tag{28}$$

where we have integrated by parts and disregarded the boundary contributions; here $\tilde{A}$ is proportional to the second nearest-neighbor interaction energy α. The contributions from the y and z derivatives have an analogous form, so that we have

$$\begin{aligned} \mathcal{F} &= \mathcal{F}_x^{(1)} + \mathcal{F}_y^{(1)} + \mathcal{F}_z^{(1)} + \mathcal{F}^{(2)} \\ &= \int_V \left[\frac{\tilde{A}}{2} \left\{ X_x^2 + Y_y^2 + Z_z^2 \right\} + \frac{\tilde{B}}{2} \left\{ |\nabla X|^2 + |\nabla Y|^2 + |\nabla Z|^2 \right\} \right] \, dV. \end{aligned} \tag{29}$$

We note that $\tilde{A} > 0$ and $\tilde{B} > 0$ follow from choosing the interaction energies to have the signs $\beta > 0$ and $\alpha > 0$; with our sign conventions, these choices are analogous to repulsive nearest-neighbor and attractive second nearest-neighbor interactions. This form of the gradient energy contribution has also been reported by Lai (1990).

2.4.3. Governing equations

The system free energy thus has the form

$$\mathcal{F} = \int \left\{ f(X,Y,Z) + \frac{A}{2}\left(X_x^2 + Y_y^2 + Z_z^2\right) + \frac{B}{2}\left(X_y^2 + X_z^2 + Y_x^2 + Y_z^2 + Z_x^2 + Z_y^2\right) \right\} dV. \quad (30)$$

A simple set of dynamical governing equations can be obtained by writing

$$\tau \frac{\partial X_j}{\partial t} = -\frac{\delta \mathcal{F}}{\delta X_j}, \quad (31)$$

where τ is a phenomenological relation parameter, which for simplicity we will take to be constant. The system then evolves along paths of steepest descent of the functional $\mathcal{F}$. Fried and Gurtin (1994) have provided alternate derivations of dynamical governing equations in related situations that are based on the second law of thermodynamics.

For equilibrium surfaces, the time derivatives are set to zero. Evaluating the functional derivatives gives

$$0 = AX_{xx} + BX_{yy} + BX_{zz} - f_X, \quad (32a)$$

$$0 = BY_{xx} + AY_{yy} + BY_{zz} - f_Y, \quad (32b)$$

$$0 = BZ_{xx} + BZ_{yy} + AZ_{zz} - f_Z. \quad (32c)$$

These are the equations we shall study in this work. The dynamic form of these equations is currently under investigation and the results will be published separately (Braun *et al.* 1995a).

3. Single phase bulk states

Equilibrium states in which the order parameters X, Y, and Z are constant require that the free-energy of the system is stationary, and hence that

$$f_X(X,Y,Z) = 2a_2X + a_3YZ + 4a_{41}X^3 + 2a_{42}X(Y^2+Z^2) = 0, \quad (33a)$$

$$f_Y(X,Y,Z) = 2a_2Y + a_3XZ + 4a_{41}Y^3 + 2a_{42}Y(X^2+Z^2) = 0, \quad (33b)$$

$$f_Z(X,Y,Z) = 2a_2Z + a_3XY + 4a_{41}Z^3 + 2a_{42}Z(X^2+Y^2) = 0. \quad (33c)$$

The stability of such equilibria may be examined by a standard linear stability analysis of the governing equations, which indicates that the stable equilibria are local minima of $f(X,Y,Z)$.

There exist distinct types of equilibria given by the solutions of Eq. (33); we now discuss the nature of the solutions as a_2 varies for fixed values of a_3, a_{41}, a_{42}.

The trivial solution $X = Y = Z = 0$ represents the disordered or fcc phase, and is stable providing $a_2 > 0$. The variable a_2 plays the role of temperature, with $a_2 = 0$ corresponding to the limit of metastability of the fcc phase.

There are solutions for which $X = \lambda \neq 0$ and $Y = Z = 0$, where

$$\lambda = \pm\sqrt{\frac{-a_2}{2a_{41}}}, \tag{34}$$

which exist only when a_2 and a_{41} have opposite sign. In this situation the order parameters may be expressed as $\rho_1 = \rho_2 = W + \lambda$ and $\rho_3 = \rho_4 = W - \lambda$, representing a layered structure consisting of planes with different copper concentrations alternating in the x-direction (c.f. Fig. 2).

We refer to this type of solution as the CuAu or $L1_0$ phase, without necessarily implying that the atoms are copper and gold or that the number of copper atoms and gold atoms are equal. Because of symmetry there are analogous solutions with $Y = \lambda$ and $X = Z = 0$, and with $Z = \lambda$ and $X = Y = 0$, that also represent the $L1_0$ phase with the layering occurring in the y and z directions. Symmetry allows changing the sign of any two of the order parameters, which allows a total of six equivalent variants of the $L1_0$ phase.

There are solutions of the form $X = Y = Z = \chi\,(\neq 0)$, where χ satisfies

$$2a_2 + a_3\chi + 4(a_{41} + a_{42})\chi^2 = 0, \tag{35}$$

which allows for two possible real values of χ, denoted χ_1 and χ_2. These solutions exist when $a_2 < a_2^L$, where

$$a_2^L \equiv \frac{a_3^2}{32(a_{41} + a_{42})}. \tag{36}$$

When $a_2 = a_2^L$, the two branches merge at a limit point where $\chi_1 = \chi_2 = -a_3/[8(a_{41} + a_{42})]$. For these solutions, $\rho_1 = W + 3\chi$ and $\rho_2 = \rho_3 = \rho_4 = W - \chi$, so that site 1 is distinguished from the other sites. We refer to this case as the $L1_2$ phase. The symmetries that correspond to changing the signs of two of the variables imply that there are related solutions of the form $X = \chi, Y = Z = -\chi$, and so forth, resulting in four variants on each of the two branches of $L1_2$ phase. A single change of sign separates the two branches; the variants have different energies, and usually do not coexist. On the Cu-Au phase diagram the different branches are designated as Cu_3Au and $CuAu_3$.

There are also "mixed-mode" solutions that bifurcate from the $L1_0$ solution branch for $a_2 < a_2^{(1)}$, where

$$a_2^{(1)} \equiv \frac{-a_{41}a_3^2}{4[2a_{41} - a_{42}]^2}\,; \tag{37}$$

they have the form

$$X = \frac{a_3}{2[2a_{41} - a_{42}]}, \qquad Y = Z = \pm\sqrt{\frac{(a_2^{(1)} - a_2)}{(2a_{41} + a_{42})}}, \tag{38}$$

and analogous solutions related by symmetry to these solutions. (If $[2a_{41} - a_{42}]$ vanishes this bifurcation point moves to infinity.) The mixed-mode and $L1_2$ solutions intersect at

$$a_2 = a_2^{(2)} \equiv \frac{(4a_{41} + a_{42})a_3^2}{2[2a_{41} - a_{42}]^2}. \tag{39}$$

The mixed-mode solutions are never stable, but play a role in determining the stability of the bulk $L1_0$ and $L1_2$ phases, as described below.

The restricted class of solutions of the governing equations Eq. (32) for which $Y = Z$ contain instances of all of the above types of equilibrium states.

If we now allow the order parameters to depend solely on time then the governing equations are

$$\tau\frac{dX}{dt} = -[2a_2X + a_3YZ + 4a_{41}X^3 + 2a_{42}X(Y^2 + Z^2)], \tag{40a}$$

$$\tau\frac{dY}{dt} = -[2a_2Y + a_3XZ + 4a_{41}Y^3 + 2a_{42}Y(X^2 + Z^2)], \tag{40b}$$

$$\tau\frac{dZ}{dt} = -[2a_2Z + a_3XY + 4a_{41}Z^3 + 2a_{42}Z(X^2 + Y^2)]. \tag{40c}$$

For the case $Y = Z$, Eq. (40) have the same form as the two-mode disturbance equations that govern the weakly nonlinear competition of rolls and hexagons in the classical Rayleigh-Benard problem of hydrodynamics (Segel 1965), as well as band-node competition in the directional solidification of a binary alloy (for a recent review, see Coriell and McFadden 1993). For the Rayleigh-Benard problem the rolls are represented by solutions of the form $X \neq 0, Y = 0$, the analogue of $L1_0$; hexagons by $X = Y\ (\neq 0)$, the analogue of $L1_2$; and the no-flow base state by $X = Y = 0$, the analogue of the disordered phase. The control parameter is the Rayleigh number, the analogue of which is the quantity $-a_2$. In the context of Rayleigh-Benard convection the solution structure of Eq. (40) is well understood and is commonly represented by a state diagram in which the amplitude

of the solutions are plotted against the Rayleigh number, which for our problem is given by $-a_2$, with all the other coefficients, a_3, a_{41} and a_{42} fixed. The nature of the solution structure depends on the values of these coefficients.

In Fig. 3 we show a schematic representation of the state diagram for the case of fixed W in

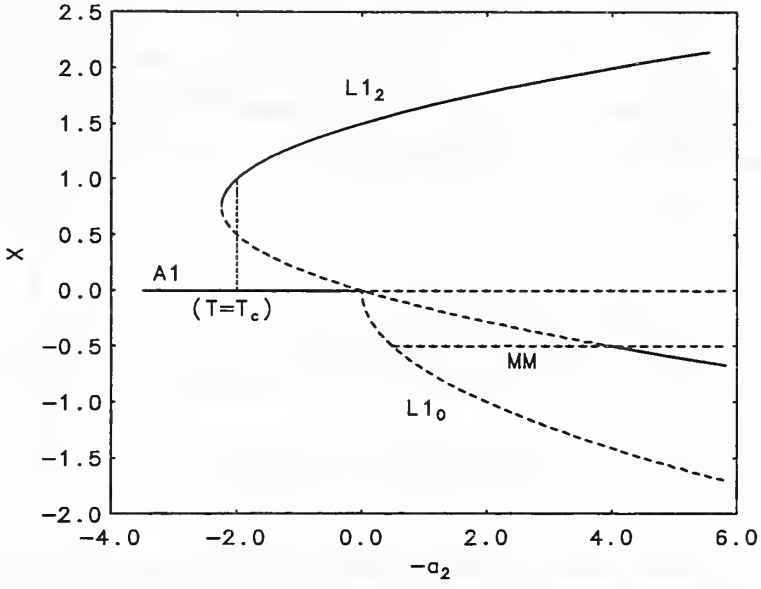

Figure 3: A schematic state diagram showing the existence of the disordered (A1), $L1_0$ and $L1_2$ bulk states, as well as the mixed-mode solution (MM), as the parameter a_2 varies. The solid and dashed lines represent stable and unstable solutions, respectively.

which a_{41} and a_{42} are both positive and $a_{42} - 2a_{41} < 0$. This diagram shows the different possible bulk states, characterised by the value of X, as a_2 is varied. It displays only half of the possible fixed W states; there are an additional set of solution branches which may be obtained from those shown by reflecting them about the abscissa, but which have been omitted here for clarity.

The abscissa in Fig. 3 represents the disordered (fcc) state $X = Y = Z = 0$; it becomes unstable for $a_2 < 0$ in a transcritical bifurcation to the $L1_2$ state and a pitchfork bifurcation to the $L1_0$ state. The $L1_2$ phases, given by $X = Y = Z$, have two values of X for a given value of $a_2 < a_2^L$. The $L1_2$ branch with larger $|X|$ is stable for $a_2 < a_2^L$; the branch with smaller $|X|$ is unstable for $a_2^L < a_2 < a_2^{(2)}$. The $L1_0$ branch is given by X negative and $Y = Z = 0$ for $a_2 > 0$; all the $L1_0$ states are unstable for $a_{42} - 2a_{41} < 0$. Lastly, there are mixed modes where only two of the order

parameters are equal but all are nonzero. They are all unstable, but they do restabilise the $L1_2$ branch for $X < 0$.

In Fig. 4 we show a schematic state diagram for the case where a_{41} and a_{42} are both positive

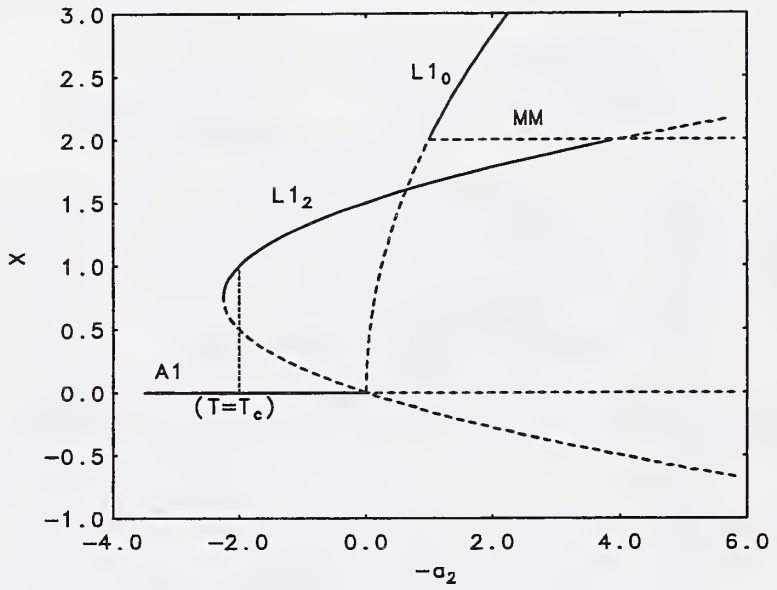

Figure 4: A schematic state diagram showing the existence of the $L1_0$ and $L1_2$ bulk states as the parameter a_2 varies. The solid (dashed) lines represent stable (unstable) solutions.

and $a_{42} - 2a_{41} > 0$. We again have the disordered (fcc) state losing stability to the $L1_2$ state in a transcritical bifurcation and to the $L1_0$ state (now $X > 0$) in a pitchfork bifurcation. However, the mixed mode now restabilises the $L1_0$ state for $X > 0$ and eventually destabilises the $L1_2$ branch. There is the possibility of bistability between both ordered states as well as between the fcc and $L1_2$ state; since W is fixed, these are points on the T_0 curves, rather than congruent points.

In terms of a phase diagram interpretation, we may regard a_2 as increasing with temperature; we may then interpret a_2^L, the minimum on the $L1_2$ branch, as corresponding to the limit of metastability of the ordered phase and $a_2 = 0$ as corresponding to the temperature of the limit of metastability of the disordered phase.

In this paper, we shall only compute solutions to the governing equations for the case $a_{42} - 2a_{41} < 0$, shown in Fig. 3. We also note that for the values of the parameters we consider, the mixed modes exist only for large values of $|X|$ (not as suggested by the schematic state diagrams) and will not

form part of our subsequent discussion.

4. Interphase boundaries

In this section we consider those one-dimensional solutions to the governing equations (32) which represent a stationary, planar, interfacial region separating an ordered $L1_2$ bulk phase from a disordered bulk phase at the same composition (usually a congruent point on a phase diagram, but in this case it is a point on the T_0 curve, since we fix W to be the same value in both phases). The order parameters vary only in a direction parallel to the unit normal to the interface, denoted by $\hat{\mathbf{n}} = (n_x, n_y, n_z)$, and so

$$X(\mathbf{x}) = \hat{X}(\hat{\mathbf{n}} \cdot \mathbf{x}),\ Y(\mathbf{x}) = \hat{Y}(\hat{\mathbf{n}} \cdot \mathbf{x}),\ Z(\mathbf{x}) = \hat{Z}(\hat{\mathbf{n}} \cdot \mathbf{x}). \tag{41}$$

The governing equations then reduce to the following system of nonlinear ordinary differential equations

$$\hat{\xi}_x^2 \hat{X}_{\zeta\zeta} = f_X(\hat{X}, \hat{Y}, \hat{Z}), \tag{42a}$$

$$\hat{\xi}_y^2 \hat{Y}_{\zeta\zeta} = f_Y(\hat{X}, \hat{Y}, \hat{Z}), \tag{42b}$$

$$\hat{\xi}_z^2 \hat{Z}_{\zeta\zeta} = f_Z(\hat{X}, \hat{Y}, \hat{Z}), \tag{42c}$$

where $\zeta = \hat{\mathbf{n}} \cdot \mathbf{x}$, and

$$\hat{\xi}_x^2 = An_x^2 + Bn_y^2 + Bn_z^2,\ \hat{\xi}_y^2 = Bn_x^2 + An_y^2 + Bn_z^2,\ \hat{\xi}_z^2 = Bn_x^2 + Bn_y^2 + An_z^2. \tag{43}$$

Assuming that the bulk disordered phase exists for $\zeta \to -\infty$ and imposes that

$$\hat{X}(\zeta),\ \hat{Y}(\zeta),\ \hat{Z}(\zeta) \to 0,\ \text{as } \zeta \to -\infty. \tag{44a}$$

We further require $a_2 > 0$ so that the bulk disordered phase is stable. We then have the ordered $L1_2$ phase as $\zeta \to +\infty$ and hence

$$\hat{X}(\zeta),\ \hat{Y}(\zeta),\ \hat{Z}(\zeta) \to \chi_1,\ \text{as } \zeta \to +\infty. \tag{44b}$$

where χ_1 represents the common value of the order parameter in the stable $L1_2$ bulk phase. The equations (42) have a first integral

$$\frac{\hat{\xi}_x^2}{2}[\hat{X}_\zeta]^2 + \frac{\hat{\xi}_y^2}{2}[\hat{Y}_\zeta]^2 + \frac{\hat{\xi}_z^2}{2}[\hat{Z}_\zeta]^2 - f(\hat{X}, \hat{Y}, \hat{Z}) = f_0 \tag{45}$$

where f_0 is a constant of integration. Inserting the far-field boundary conditions (44) into this expression gives that

$$f_0 = f(\chi_1, \chi_1, \chi_1) = f(0,0,0) = 0; \tag{46}$$

since $f(0,0,0) = 0$, i.e., the free-energy of each of the bulk phases must be equal. From the form of the free-energy density, this requires that

$$3a_2 + a_3\chi_1 + 3(a_{41} + a_{42})\chi_1^2 = 0. \tag{47}$$

Combined with Eq. (35), the equation for χ_1, this gives that

$$\chi_1 = -\frac{6a_2}{a_3}, \tag{48}$$

and

$$(a_3)^2 = 36a_2(a_{41} + a_{42}). \tag{49}$$

We note that this condition allows the $L1_2$ and disordered phases to coexist in stable equilibrium only for a unique value of a_2.

Let $a_2^\star, a_3^\star, a_{41}^\star$ and $a_{42}^\star$, denote the values of the a_2, a_3, a_{41} and a_{42} which satisfy Eq. (49) for the existence of an interphase boundary, and let $\chi^\star$ denote the corresponding value of the order parameters in the $L1_2$ bulk phase given by Eq. (48), i.e., $\chi^\star = -6a_2^\star/a_3^\star$. Nondimensionalising the governing equations

$$\hat{X}(\zeta) = \chi^\star \tilde{X}(\tilde{\zeta}), \quad \hat{Y}(\zeta) = \chi^\star \tilde{Y}(\tilde{\zeta}), \quad \hat{Z}(\zeta) = \chi^\star \tilde{Z}(\tilde{\zeta}), \tag{50a}$$

$$\zeta = \frac{1}{\chi^\star}\sqrt{\frac{A}{a_{41}}}\tilde{\zeta}, \quad f(\hat{X}, \hat{Y}, \hat{Z}) = [\chi^\star]^4 a_{41} \tilde{f}(\tilde{X}, \tilde{Y}, \tilde{Z}). \tag{50b}$$

Here

$$\tilde{f}(\tilde{X}, \tilde{Y}, \tilde{Z}) = \tilde{a}_2(\tilde{X}^2 + \tilde{Y}^2 + \tilde{Z}^2) + \tilde{a}_3\tilde{X}\tilde{Y}\tilde{Z} + (\tilde{X}^4 + \tilde{Y}^4 + \tilde{Z}^4) + \tilde{a}_{42}(\tilde{X}^2\tilde{Y}^2 + \tilde{X}^2\tilde{Z}^2 + \tilde{Z}^2\tilde{Y}^2), \tag{51}$$

where

$$\tilde{a}_2 = \frac{a_2(a_3^\star)^2}{36a_{41}(a_2^\star)^2}, \quad \tilde{a}_3 = -\frac{a_3 a_3^\star}{6a_{41}a_2^\star}, \quad \tilde{a}_{42} = \frac{a_{42}}{a_{41}}. \tag{52}$$

In terms of these parameters an interphase boundary forms when $a_2 = a_2^\star, a_3 = a_3^\star$ etc, and so, on using Eq. (49) we find

$$\tilde{a}_2 = -\frac{\tilde{a}_3}{6} = 1 + \tilde{a}_{42}. \tag{53}$$

We define the unique value of $\tilde{a}_2$ for coexistence as

$$\tilde{a}_2^c \equiv 1 + \tilde{a}_{42}. \tag{54}$$

Finally, we define

$$\xi_x^2 = n_x^2 + \epsilon^2 n_y^2 + \epsilon^2 n_z^2,\ \xi_y^2 = \epsilon^2 n_x^2 + n_y^2 + \epsilon^2 n_z^2,\ \xi_z^2 = \epsilon^2 n_x^2 + \epsilon^2 n_y^2 + n_z^2, \tag{55}$$

where $\epsilon^2 = B/A$.

We henceforth omit the tilde's on the dimensionless quantities; the dimensionless governing equations are then

$$\xi_x^2 X_{\zeta\zeta} = f_X(X,Y,Z), \tag{56a}$$

$$\xi_y^2 Y_{\zeta\zeta} = f_Y(X,Y,Z), \tag{56b}$$

$$\xi_z^2 Z_{\zeta\zeta} = f_Z(X,Y,Z), \tag{56c}$$

with boundary conditions

$$X(\zeta),\ Y(\zeta),\ Z(\zeta) \to 0,\ \text{as}\ \zeta \to -\infty, \tag{57a}$$

$$X(\zeta),\ Y(\zeta),\ Z(\zeta) \to 1,\ \text{as}\ \zeta \to +\infty. \tag{57b}$$

The interfacial energy γ is given by the excess free energy per unit area, which may be written as

$$\gamma = \int_{-\infty}^{\infty} \left\{ \frac{\xi_x^2}{2}[X_\zeta]^2 + \frac{\xi_y^2}{2}[Y_\zeta]^2 + \frac{\xi_z^2}{2}[Z_\zeta]^2 + f(X,Y,Z) \right\} d\zeta; \tag{58}$$

here $(X(\zeta), Y(\zeta), Z(\zeta))$ denotes the solution to equations (56) and (57). By using the first integral (45), the interfacial energy may be expressed in either of the equivalent forms

$$\gamma = \int_{-\infty}^{\infty} \left\{ \xi_x^2[X_\zeta]^2 + \xi_y^2[Y_\zeta]^2 + \xi_z^2[Z_\zeta]^2 \right\} d\zeta = 2\int_{-\infty}^{\infty} f(X,Y,Z) d\zeta. \tag{59}$$

The interfacial energy of the layer solution can also be regarded as the extremal value for a variational formulation of the one-dimensional governing equations (56); they are the Euler equations for the variational problem

$$\gamma = \min \int_{-\infty}^{\infty} \left\{ \frac{\xi_x^2}{2}[X_\zeta]^2 + \frac{\xi_y^2}{2}[Y_\zeta]^2 + \frac{\xi_z^2}{2}[Z_\zeta]^2 + f(X,Y,Z) \right\} d\zeta, \tag{60}$$

where the minimum is taken over all functions $(X(\zeta), Y(\zeta), Z(\zeta))$ satisfying the boundary conditions (57).

4.1. Geodesic interpretation

A geometric interpretation of the one-dimensional layer solutions is possible in terms of geodesic curves, $(X(\zeta), Y(\zeta), Z(\zeta))$ that minimise a generalised distance between the points $(0,0,0)$ and $(1,1,1)$ (see, e.g., Sternberg 1991). Using the inequality $2ab \leq a^2 + b^2$ in the expression (60), gives

$$\gamma \geq \min \int_{-\infty}^{\infty} \sqrt{2\, f(X,Y,Z)} \sqrt{\xi_x^2 [X_\zeta]^2 + \xi_y^2 [Y_\zeta]^2 + \xi_z^2 [Z_\zeta]^2}\, d\zeta, \tag{61}$$

and from the first integral Eq. (45) of the layer solution, the inequality is actually an equality. If we define a weighted arclength on curves $(X(\zeta), Y(\zeta), Z(\zeta))$ by $ds^2 = \xi_x^2 dX^2 + \xi_y^2 dY^2 + \xi_z^2 dZ^2$, this expression can be written in the form

$$\gamma = \min \int_{(0,0,0)}^{(1,1,1)} \sqrt{2\, f(X,Y,Z)}\, ds; \tag{62}$$

that is, the interfacial energy γ can be viewed as the geodesic distance between the points $(0,0,0)$ and $(1,1,1)$ in a metric given by the integral of $\sqrt{2\, f(X,Y,Z)}$ with respect to the arclength ds. The layer solution is the corresponding geodesic curve. In special cases in which the path of the geodesic can be inferred from symmetry considerations, e.g., if only a single non-zero order parameter is involved in the transition, an explicit expression for the surface energy can thus be obtained immediately by quadrature.

4.2. Numerical and asymptotic solutions

In the computations of interphase boundaries presented below we set $a_2 = a_2^c = 2, a_3 = -12, a_{42} = 1$, which satisfies the relation given by Eq. (53). To ensure the accuracy of our numerical solutions we have used two methods to compute solutions of the nonlinear system of ordinary differential equations, Eq. (56), with the boundary conditions Eq. (57a) and Eq. (57b). In the first approach we employed a central finite difference approximation to the spatial derivatives and solved the resulting nonlinear algebraic equations by Newton's method, allied with a continuation method to provide suitable initial guesses. The second approach used the software package COLNEW (Bader and Ascher 1987) which solves nonlinear boundary value problems. The package employs adaptive meshing on a variable number of subintervals, with the solution on each subinterval approximated by a convenient set of algebraic basis vectors. The resulting solutions for the coefficients of the basis vectors of the basis vectors allow accurate evaluation of the solution wherever desired in the interval.

We note from the state diagrams for the values of the parameters used in the computations, e.g. Fig. 3, that the $L1_0$ forms a supercritical bifurcation from the disordered phase; hence, both these bulk phases cannot be stable for the same value of a_2. This does not allow the possibility of an IPB between the disordered and $L1_0$ bulk phases.

4.3. The orientation dependence

We now go on to discuss the dependence of the interfaces on their orientation. Because of the underlying $m\bar{3}m$ symmetries of the $L1_2$ and the disordered fcc, only those orientations whose normals $\hat{\mathbf{n}}$ are subtended by the spherical triangle whose vertices are given by the intersection of the unit sphere and radial vectors in the directions of $\hat{\mathbf{n}}$, [100], [110] and [111] need to be considered. The $m\bar{3}m$ symmetry dictates that scalar properties, such as the surface energy, will have extrema at $< 111 >$ and $< 100 >$, an extremum or saddle at $< 110 >$, and no gradients normal to the sides of the spherical triangle.

We first discuss solutions for special orientations for which symmetry imposes relationships among the order parameters, and then go on to general interface orientations for which there are no such relationships. The only symmetry operations in $m\bar{3}m$ that impose such relationships are the $\{110\}$ mirrors and the $\bar{3}$ axes along $< 111 >$. For an IPB in the (111) plane, with $\hat{\mathbf{n}}$ along [111], we have one-dimensional solutions of the form $X(\zeta) = Y(\zeta) = Z(\zeta)$. Two of the order parameters are equal for any surface that contains a $< 110 >$, or, equivalently, any $\hat{\mathbf{n}}$ lying in a $\{110\}$ mirror for which the magnitudes of two of the components of $\hat{\mathbf{n}}$ are equal. For any other orientation there is no relationship among the order parameters. These include the $\hat{\mathbf{n}} =< hk0 >$ that lie on the cube plane, except for the $< 100 >$ and $< 110 >$.

4.3.1. The isotropic IPB and the [111] IPB

We begin by considering two cases together. The first is the isotropic case in which $A = B$ (or $\epsilon = 1$) for an arbitrarily oriented interface. The other is the anisotropic case ($A \neq B$, $\epsilon \neq 1$) with $\hat{\mathbf{n}}$ oriented in the [111] direction ($n_x = n_y = n_z = 1/\sqrt{3}$). In both these cases $\xi_x = \xi_y = \xi_z$, and there are one-dimensional solutions of the form $X(\zeta) = Y(\zeta) = Z(\zeta)$ that represent $L1_2$ throughout the interfacial layer. The governing equations (56) give, on using Eq. (53), that

$$\xi^2 X_{\zeta\zeta} = 4a_2 X(1 - X)(1/2 - X), \tag{63}$$

where $\xi^2 = 1$ for the isotropic case and $\xi^2 = (1 + 2\epsilon^2)/3$ for the [111] case. This has solution

$$X(\zeta) = \frac{1}{2}\left\{1 + \tanh\left(\frac{\sqrt{2a_2}\zeta}{2\xi}\right)\right\}. \tag{64}$$

In the geodesic interpretation, the solution is a straight line segment connecting the points $(0,0,0)$ and $(1,1,1)$ in the space of points (X,Y,Z). In Fig. 5 we display the corresponding sublattice

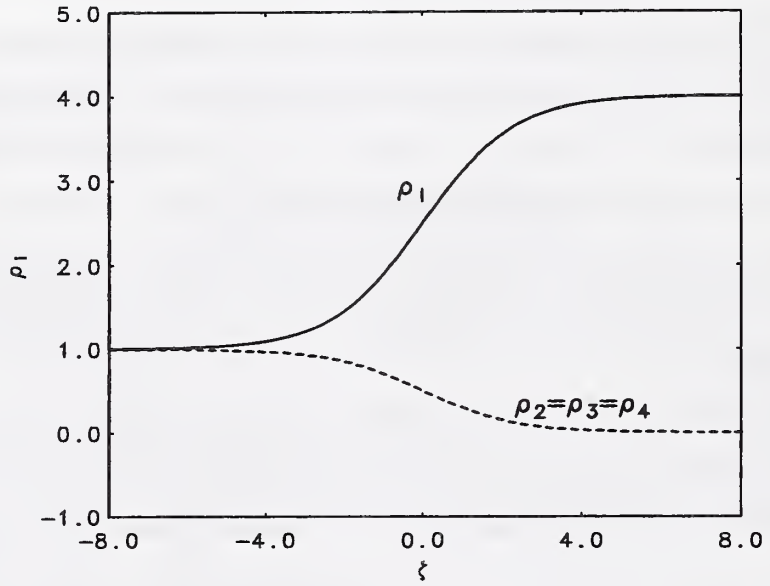

Figure 5: The sublattice atomic fractions for $a_{42} = 1$ and $\epsilon^2 = 0.005$ for the [111] IPB. Note that $X = Y = Z$ for this orientation.

atomic fractions as functions of ζ; the interface clearly consists of a $L1_2$ structure in which the atomic fractions of three of the sublattices are the same at each station and distinguished from the remaining sublattice.

4.3.2. The special $\hat{\mathbf{n}}$ in $\{110\}$ mirrors

Interfaces with normals of the form $< hkk >$ span the two sides of the spherical triangle that run from [111] to either [100] with $h > k$, or to [110] with $h < k$. In contrast, the interfaces represented by the third side, the $< hk0 >$ running along the cube mirror plane from [100] to [110], have no special symmetry relations for these computations.

For an interface oriented in the [100] direction ($n_x = 1$ and $n_y = n_z = 0$), we have $\xi_x^2 = 1$ and $\xi_y^2 = \xi_z^2 = \epsilon^2$. There are one-dimensional solutions with $Y(\zeta) = Z(\zeta)$, in which case Equations (56)

become

$$X_{\zeta\zeta} = 2a_2X + a_3Y^2 + 4\left(X^2 + a_{42}Y^2\right)X, \tag{65a}$$

$$\epsilon^2 Y_{\zeta\zeta} = 2a_2Y + a_3XY + 2\left([2 + a_{42}]Y^2 + a_{42}X^2\right)Y. \tag{65b}$$

Computed solutions of this system are shown in Figures 6 and 7 for $\epsilon^2 = 0.005$. Fig. 6 shows a

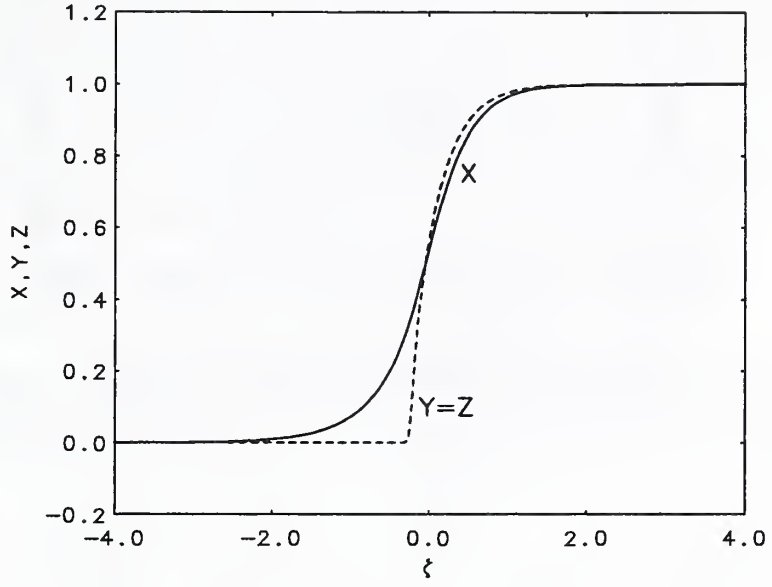

Figure 6: The order parameters for $a_{42} = 1$ and $\epsilon^2 = 0.005$ for the [100] IPB. Note that $Y = Z$ for this orientation.

"delay" in the increase of Y from zero compared to X. In the (X, Y) plane, the geodesic connecting the points $(1, 1)$ and $(0, 0)$ is roughly described by an arc from the point $(1, 1)$ to a point $(X_c, 0)$ on the axis $Y = 0$, followed by a line segment from $(X_c, 0)$ to the origin $(0, 0)$.

As can be seen clearly from the corresponding plot of the sublattice atomic fractions shown in Fig. 7 this results in a region within the interfacial layer where there are just two distinct pairs of sublattices, each sublattice of the pair having the same atomic fraction of Au. This region is therefore occupied by the $L1_0$ phase, although this is not a stable bulk phase.

This interesting layered structure of the interface was first found by Kikuchi and Cahn (1979) in their cluster variation simulation of the copper-gold alloy; recently, more refined calculations have been carried out by Finel *et al.* (1990, 1992). In those models, the composition was allowed to vary across the interface, unlike our simpler model. In Fig. 8 we reproduce the corresponding result of

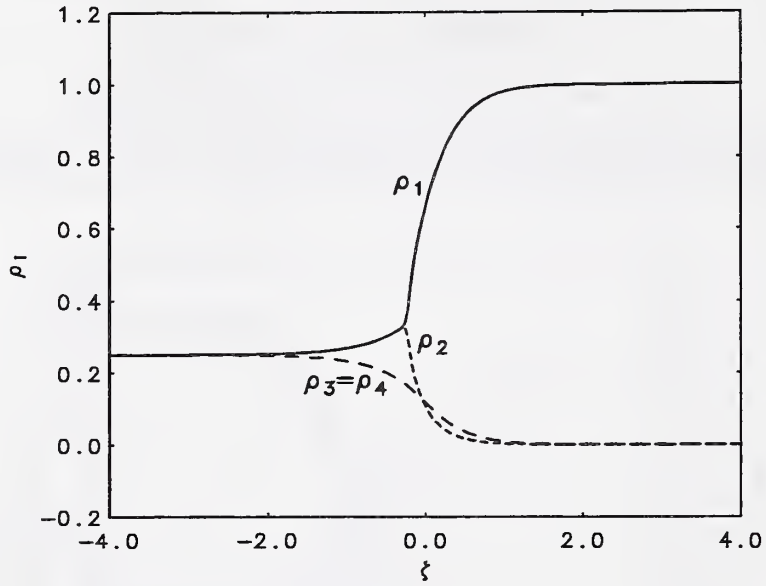

Figure 7: The sublattice occupation densities ρ_i for $a_{42} = 1$ and $\epsilon^2 = 0.005$ for the [100] IPB.

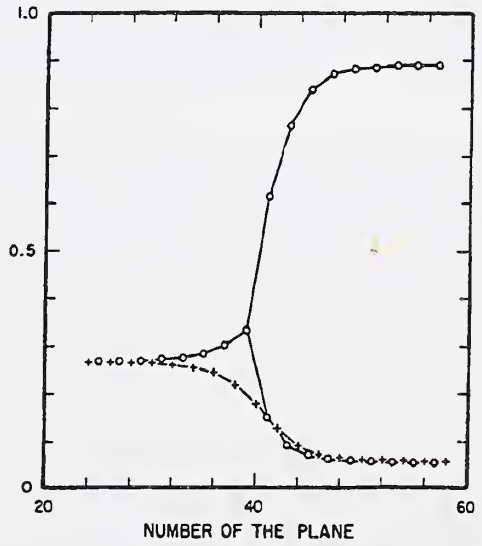

Figure 8: The interfacial structure predicted by Kikuchi and Cahn (1979) for the [100] IPB (their figure 11(b)); the curves represent the various occupation densities of the lattice as in Figure 7.

Kikuchi and Cahn, which shows the occupation densities of the 4 sublattices of the (spatially discrete) cluster variation method plotted against distance through the interfacial layer. Comparison of Fig. 7 and Fig. 8 shows the striking qualitative agreement between our work and theirs. While our result is not directly analogous with theirs, our more restricted model appears to retain the essence of the interfacial layering. It is interesting to note that layering in interfaces between phases has been observed in the molecular dynamics computations by Landman *et al.* (1980,1981) and Cleveland *et al.* (1982), though in that context the layering is strictly onto a lattice arrangement for a pure material (see also Cahn and Kikuchi 1985).

For the [110] case $n_x = n_y = 1/\sqrt{2}$ and $n_z = 0$ and have $\xi_x^2 = \xi_y^2 = (1+\epsilon^2)/2$ and $\xi_z^2 = \epsilon^2$. We then have $X(\zeta) = Y(\zeta)$ and the governing equations Eq. (53) become

$$\xi_x^2 X_{\zeta\zeta} = 2a_2 X + a_3 X Z + X\left(2[2+a_{42}]X^2 + 2a_{42}Z^2\right), \tag{66}$$

$$\xi_z^2 Z_{\zeta\zeta} = 2a_2 Z + a_3 X^2 + 4\left(2Z^2 + a_{42}X^2\right) Z. \tag{67}$$

Computed spatial profiles for the [110] orientation are shown in Figures 9. The strong separation

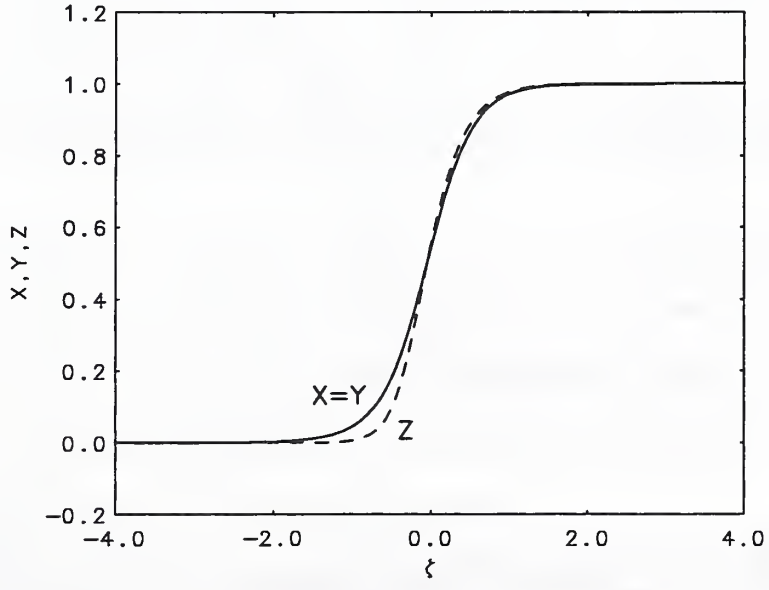

Figure 9: The order parameter variation for $a_{42} = 1$ and $\epsilon^2 = 0.005$ for the [110] IPB. Note that $X = Y$ for this orientation.

of layer widths which occurred for the [100] orientation does not occur here; as a consequence no interfacial layering occurs. When the order parameters are converted to the occupation densities,

there is again striking agreement with the computed results of Kikuchi and Cahn (1979, see their Figure 15).

No significant change is needed to calculate the solution for all the orientations along the two sides of the spherical triangle that include all the $< hkk >$. We fixed all the parameters but the orientation; in particular we choose $\epsilon^2 = 0.005$ to ensure the formation of the $L1_0$ interfacial layer in the [100] direction. For the orientations represented by the side of the spherical triangle between the [111] and [100] vertices $Y(\zeta) = Z(\zeta)$; but $X(\zeta)$ separates from them with increasing distance from [111]. In fact, the symmetry of the equations for these orientations is the same as for the [100] direction, Eq. (65), because the Y and Z equations are identical. Moreover, it may be shown that the $L1_0$ layering observed in the limit $\epsilon \to 0$ is only apparent for orientations sufficiently close to the [100] direction for which the azimuthal angle, ϕ, is $\mathcal{O}(\epsilon)$. In our computations with $\epsilon^2 = 0.005$ the formation of the $L1_0$ layer becomes apparent for $\phi \approx 25°$, which is $\phi \approx 4\epsilon$ radians. An example of the solution on this side of the spherical triangle for $\phi = 18.25°$ is given in Fig. 10.

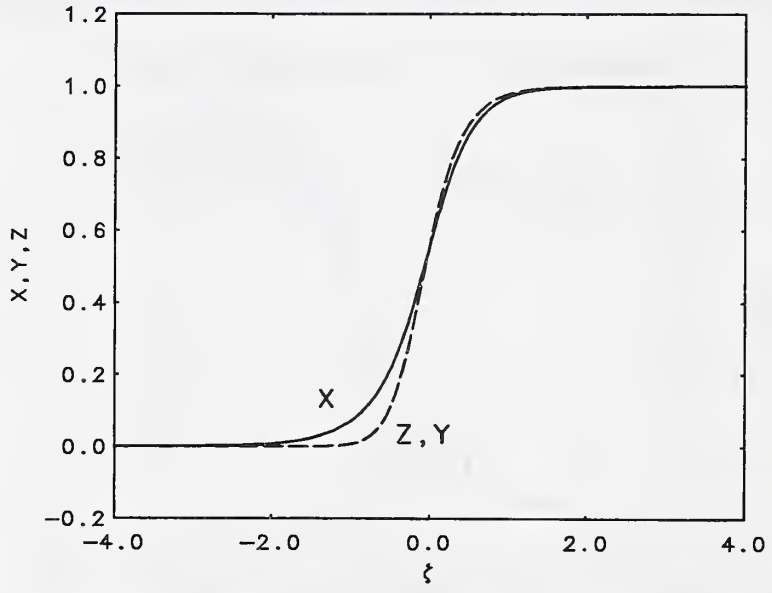

Figure 10: The order parameter variation for $a_{42} = 1$, $\epsilon^2 = 0.005$, azimuthal angle $\phi = 18.25°$, and polar angle $\theta = 72.16°$ on the upper side of the spherical triangle.

Varying the orientations from the [111] vertex to the [110] reveals behavior analogous with the [110], with $X(\zeta) = Y(\zeta)$ and $Z(\zeta)$ separating from them as the orientations are moved away from the [111] direction. The results are very similar to those shown in Fig. 9.

4.3.3. General orientations

We have also computed the solutions of the governing equations, (56) for general orientations of a planar interface with respect to the crystal axes. Within the spherical triangle the $X(\zeta)$, $Y(\zeta)$ and $Z(\zeta)$ are also all distinct. A typical solution is shown in Fig. 11 for $\theta = 80°$ and $\phi = 35°$. General

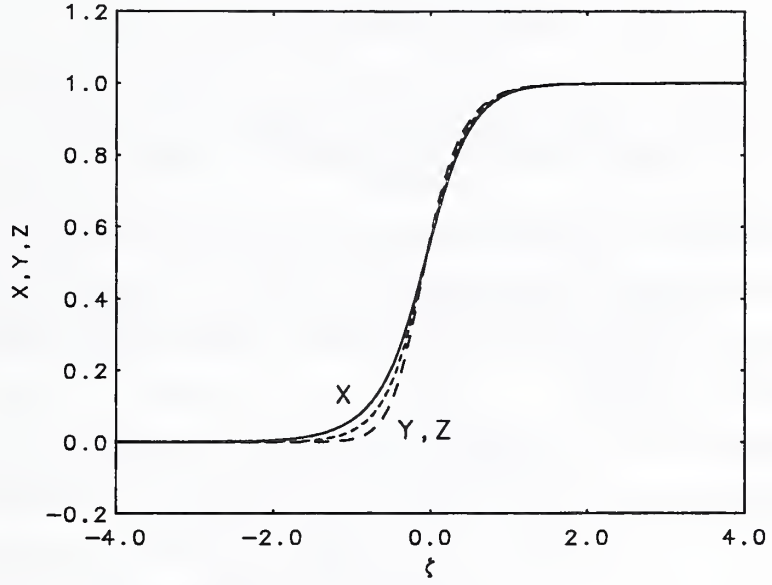

Figure 11: The order parameter variation for $a_{42} = 1$, $\epsilon^2 = 0.005$, azimuthal angle $\phi = 35°$ and polar angle $\theta = 80°$ away from the edges of the spherical triangle.

orientations include the open interval of the side of the spherical triangle connecting the [100] and [110] vertices for which the $X(\zeta)$, $Y(\zeta)$ and $Z(\zeta)$ are all distinct. Along that side, as the orientation varies away from the [100] direction, the Z component separates from its like component Y and finally becomes the same as the X component as the orientation approaches [110].

4.3.4. The asymptotic limit $\epsilon \to 0$ for the [100] IPB

To help understand some of the mathematical aspects of the [100] IPB layering, we now seek a solution asymptotic to the computed solutions of the governing equations (65) in the limit of $\epsilon \to 0$.

An outer solution that is a regular perturbation series as $\epsilon \to 0$ is:

$$X = X^{(0)}(\eta) + \epsilon^2 X^{(1)}(\eta) + \mathcal{O}(\epsilon^4), \;\; Y = Y^{(0)}(\eta) + \epsilon^2 Y^{(1)}(\eta) + \mathcal{O}(\epsilon^4). \tag{68}$$

The leading order problem is then

$$X^{(0)}_{\eta\eta} = 2a_2X^{(0)} + a_3(Y^{(0)})^2 + 4[(X^{(0)})^2 + a_{42}(Y^{(0)})^2]X^{(0)}, \tag{69}$$

$$0 = Y^{(0)}\left[2a_2 + a_3X^{(0)} + 2[2 + a_{42}](Y^{(0)})^2 + 2a_{42}(X^{(0)})^2\right]. \tag{70}$$

Solving (70),

$$Y^{(0)} \equiv 0,\ X^{(0)}(\eta) < X_c \tag{71}$$

or

$$Y^{(0)} = \pm\sqrt{-\frac{2a_2 + a_3X^{(0)} + 2a_{42}(X^{(0)})^2}{2[2 + a_{42}]}},\ X^{(0)}(\eta) > X_c; \tag{72}$$

at $X^{(0)} = X_c$, the numerator of the radical vanishes. Because solutions to (69) and (70) are translationally invariant, we are free to choose η such that $X^{(0)}(0) = X_c$. Thus the regular perturbation series generates two outer solutions valid on two domains: Region I where $X^{(0)} < X_c$ ($\eta < 0$) and Region II where $X^{(0)} > X_c$ ($\eta > 0$).

The order parameter $X^{(0)}(\eta)$ is required to evaluate $Y^{(0)}$; the leading-order solution for $X^{(0)}$ is, for $X^{(0)}(\eta) < X_c$,

$$X^{(0)}(\eta) = \frac{-\sqrt{a_2}}{\sinh[\sqrt{2a_2}(\eta - \eta_I)]}. \tag{73}$$

For $X^{(0)}(\eta) > X_c$,

$$X^{(0)}(\eta) = 1 - \frac{\beta_3}{\alpha + \beta_1\sinh\beta_2(\eta - \eta_{II})},\ \text{if } 2\alpha^2 < 1; \tag{74}$$

or

$$X^{(0)}(\eta) = 1 - \frac{\beta_3}{\alpha + \beta_1\cosh\beta_2(\eta - \eta_{II})},\ \text{if } 2\alpha^2 > 1, \tag{75}$$

with

$$\alpha = \frac{3 + a_2}{\sqrt{(3 + 2a_2)|3 - a_2|}},\ \beta_1 = \sqrt{|1/2 - \alpha^2|},\ \beta_2 = \sqrt{\frac{2a_2(3 + 2a_2)}{1 + a_2}},\ \beta_3 = \sqrt{\frac{3 + 2a_2}{|3 - a_2|}}, \tag{76}$$

where Eq. (53) has been used to express these quantities solely in terms of a_2; η_I and η_{II} are constants of integration that are as yet undetermined. We note from Eq. (72) that $Y^{(0)} \propto \sqrt{\eta}$ as $\eta \to 0^+$, and hence it has an unbounded second derivative as $\eta \to 0^+$. This suggests we require an inner region, between the outer regions I and II, which will take account of the second derivative of Y. The inner region also acts to relate the two outer solutions and hence determines the constants η_I and η_{II}.

We now investigate the inner problem by introducing the rescaled distance in the inner region, ρ, defined by $\eta = \rho\epsilon^{2/3}$, and expanding the solution as

$$X(\eta) = x(\rho) = x^{(0)}(\rho) + \epsilon^{2/3}x^{(1)}(\rho) + \mathcal{O}(\epsilon), \tag{77}$$

and

$$Y(\eta) = y(\rho) = \epsilon^{1/3}\left[y^{(0)}(\rho) + \epsilon^{2/3}y_1(\rho) + \mathcal{O}(\epsilon)\right], \tag{78}$$

which balances the second derivative of y with the cubic nonlinearity and will allow matching to the outer solutions. Substituting these forms in the governing equations and matching to the outer solutions requires that

$$x^{(0)}(\rho) = X_c \text{ and } x^{(1)}(\rho) = D_1\rho, \tag{79}$$

where D_1 is a constant. Matching to the outer solution for X shows that

$$X^{(0)}(0^-) = X^{(0)}(0^+) = X_c \text{ and } \left.\frac{dX^{(0)}}{d\eta}\right|_{\eta=0^+} = \left.\frac{dX^{(0)}}{d\eta}\right|_{\eta=0^-} = D_1, \tag{80}$$

and so the outer solution for $X^{(0)}$ and its first derivative are continuous across the inner region, which in turn determine η_I and η_{II}.

The equation for the leading-order inner solution for y is

$$y^{(0)}_{\rho\rho} = (4X_c - 12)(X_C + D_1\rho)y^{(0)} + 6(y^{(0)})^3, \tag{81}$$

with matching conditions

$$y^{(0)} \to 0, \text{ as } \rho \to -\infty, \tag{82a}$$

$$y_0 \to \rho^{1/2}\sqrt{\frac{2D_1(X_c - 3)}{3}}, \text{ as } \rho \to +\infty. \tag{82b}$$

This provides a description of the leading-order variation of Y in the inner region. From Eq. (77) and Eq. (78) we note that in the inner region X is non-zero ($X = \mathcal{O}(1)$) and Y is almost zero ($Y = Z = \mathcal{O}(\epsilon^{2/3})$) indicating that the inner region is composed of $L1_0$ material, as suggested by the numerical solutions.

We may use this asymptotic form of the solution in the expression for the interfacial energy to obtain

$$\gamma = \sqrt{2}\left\{\int_0^{X_c}\sqrt{f(X_0,0,0)}dX_0 + \int_{X_c}^{1}\sqrt{f(X^{(0)},Y^{(0)},Y^{(0)})}dX_0\right\} + \mathcal{O}(\epsilon^{2/3}). \tag{83}$$

ϵ	γ
0.3740	0.607343
0.1000	0.537039
0.0374	0.527107
0.0100	0.525863

Table 1: The interfacial energy, γ, computed from eqn. (84) using the trapezoidal rule and numerical solutions to the governing equations computed using the software package COLNEW. Here $a_2 = 2$, $a_3 = -12$ and $a_{42} = 1$. The asymptotic result as $\epsilon \to 0$ is $\gamma = 0.525553 + \mathcal{O}(\epsilon^{2/3})$.

Note that the leading-order behaviour of the interfacial energy is independent of the leading-order solution for Y in the inner region and so we do not numerically compute $y^{(0)}$ from Eq. (81). However, the first integral in Eq. (83) may be integrated directly and the integrand of the second can be displayed explicitly to give

$$\gamma = \sqrt{2}\left\{\frac{1}{3}(a_2 + X_c^2)^{3/2} - a_2^{3/2} + \int_{X_c}^{1}(X_0 - 1)\sqrt{[(3-a_2)X_0^2 + 4a_2X_0 - a_2]}\,dX_0\right\}. \qquad (84)$$

We compute the leading order approximation to the interfacial energy to be 0.525553. In Table 1 we tabulate the interfacial energy computed from a numerical solution of the governing equations for different values of ϵ, showing that as ϵ decreases the interfacial energy approaches the leading-order value.

A heuristic explanation for the observed structure of the $L1_0$ intermediate layer that is obtained for $\epsilon \ll 1$ can also be given in terms of the geodesic interpretation. When $Y = Z$, then $g(X,Y) = f(X,Y,Y)$, and the variational principle has the form

$$0 = \delta \int_{(0,0)}^{(1,1)} \sqrt{2g(X,Y)}\,\sqrt{dX^2 + 2\epsilon^2 dY^2}. \qquad (85)$$

In the spirit of the Γ-convergence approach (De Giorgi 1978), we consider the leading order behavior expected for $\epsilon \ll 1$ by setting $\epsilon = 0$ in the weighted arc length, which becomes simply $ds = dX$. For solutions of the form $Y = Y(X)$ with $Y(0) = 0$ and $Y(1) = 1$, the leading order behavior is described by the reduced problem

$$0 = \delta \int_0^1 \sqrt{2g(X,Y)}\,dX, \qquad (86)$$

whose solution must satisfy $g_Y(X,Y)\delta Y = 0$. This is equivalent to the leading order equation (70) satisfied by the outer solution, and, as noted above, the solutions are given by Eq. (72) and the

curve $Y = 0$. The shortest distance to the origin from the point $(1, 1)$ is then obtained by using the solution $Y = Y(X)$ to Eq. (72) for $X_c \leq X \leq 1$ that satisfies $Y(1) = 1$ and $Y(X_c) = 0$, followed by the solution $Y = 0$ for $0 \leq X \leq X_c$, which represents the intervening $L1_0$ layer.

4.3.5. Interfacial energy

From our numerical solutions we have evaluated the interfacial energy as a function of interface orientation. Figure 12 shows contours of the interfacial energy on the unit sphere for $\epsilon^2 = 0.005$.

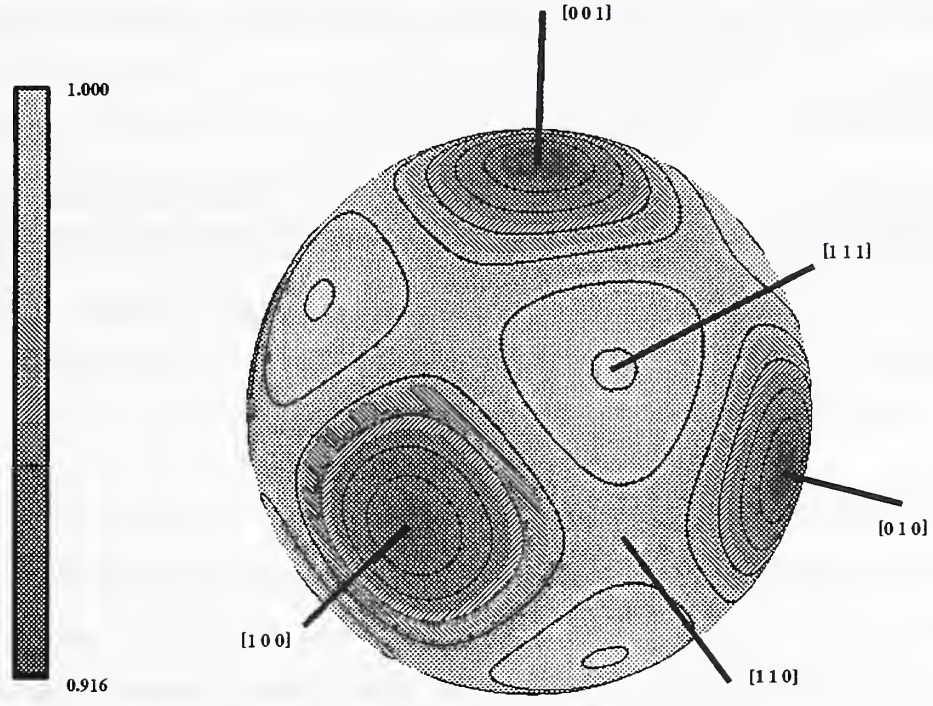

Figure 12: The variation of surface energy on the unit sphere for $a_{42} = 1$ and $\epsilon^2 = 0.005$.

The interfacial energy has a global maximum in the [111] direction and a global minimum in the [100] direction; in the [110] direction, there is a saddle point. This behaviour of the interfacial

energy shows the expected $m\bar{3}m$ symmetry. Our findings are consistent with Kikuchi and Cahn's (1979) finding of the ranking $\gamma_{100} < \gamma_{110}$. It is natural to ask whether the equilibrium shapes will develop missing orientations; a two-dimensional ordered particle with interfacial energy of the form $\gamma_0 + \gamma_4 \cos 4\theta$ would not develop corners with the level of anisotropy we have found at $\epsilon^2 = 0.005$. In order to study the three dimensional case, we adopt the vector thermodynamics formalism of Hoffman and Cahn (1972) and Cahn and Hoffman (1974) and use the "ξ-vector" to determine the equilibrium shapes given the anisotropy of interfacial energy. We computed ξ in cartesian coordinates; see e.g., the appendix of Voorhees *et al.* (1984). For $\epsilon^2 = 0.005$, the equilibrium shape determined from the interfacial energy shown in Figure 12 does not develop missing orientations. While the anisotropy of the interfacial energy is relatively weak, the equilibrium shape has definitely developed a rounded cuboidal shape with no angular edges, even for the highest anisotropies studied.

5. Antiphase boundaries

An antiphase boundary separates two variants of the $L1_2$ phase that necessarily share the same free energy, and can be expected to exist for a range of values of $a_2 < a_2^L$, where a_2^L is the value of a_2 at the limit point of the $L1_2$ branch (see Fig. 3). This is in contrast to interphase boundaries that only exist when $a_2 = a_2^c$; that is, where the free energy of the $L1_2$ and disordered fcc bulk phases are equal. For the parameters chosen here, recall that $a_2^c = 2$ and $\chi_1 = 1$.

5.1. The orientation dependence

Antiphase boundaries separate two ordered ($L1_2$) domains that are shifted by a $(1/2) < 110 >$ vector relative to one another. Because this shift breaks the cubic symmetry, it matters which vector is chosen from this set of vectors. Take $(1/2)[101]$ as an example; the y direction is then the distinguished direction and remains as the common 4-fold axis that threads both domains. For a $(1/2)[110]$ shift the z direction becomes the tetragonal axis. These cases are related by an appropriate rotation. For symmetry arguments and in the presentation of orientation dependencies we will always take the z axis as the unique 4-fold axis.

For a $(1/2)[110]$ shift the atomic fractions of the two ordered domains are given respectively by $\rho_1 = W + 3\chi, \rho_2 = \rho_3 = \rho_4 = W - \chi$ for one and $\rho_4 = W + 3\chi, \rho_1 = \rho_2 = \rho_3 = W - \chi$ for the other, and the domains are differentiated by the distinguished atomic fractions on sublattices 1 and 4. The

shift changes the sign of two of the order parameters; $X = Y = Z = \chi$ and $-X = -Y = Z = \chi$, respectively. Without loss of generality, we will consider this type of shift in our calculations of the structure of antiphase boundaries for all the orientations.

The resultant symmetry of the orientational properties of the APB is $4/mmm$, a thirding subgroup of $m\bar{3}m$. For this group of order 16, the spherical triangle has corners at the [001] (a 4-fold axis), at the [100] (no longer a 4-fold axis) and at the [110] two-fold axes, and encompasses three of the $m\bar{3}m$ triangles. This symmetry dictates that scalar properties, such as the surface energy, will have an extremum at $< 001 >$, extrema or saddles at $< 100 >$ and $< 110 >$, and no gradients normal to the sides of this larger triangle.

Most of the {110} mirrors that were important in the IPB calculations have been lost. The only special orientations for the computations are the [hhk] (but not the [khk]) that lie in the $(1\bar{1}0)$ mirror plane for which $X = Y$. In particular, for the [111] orientation, this is the only symmetry that applies. All orientations other than the [hhk], including [100], are general orientations with distinct values for X, Y, and Z.

The dimensionless governing equations are given by Eq. (56), but with boundary conditions

$$X(\zeta),\, Y(\zeta) \to -\chi_1,\; Z(\zeta) \to +\chi_1 \text{ as } \zeta \to -\infty, \tag{87}$$

and

$$X(\zeta),\, Y(\zeta),\, Z(\zeta) \to +\chi_1, \text{ as } \zeta \to +\infty, \tag{88}$$

where χ_1 is the dimensionless value order parameters in the bulk states, which is given from Eq. (35) as the positive root of

$$2a_2 + a_3\chi + 4(1 + a_{42})\chi^2 = 0. \tag{89}$$

Below we discuss dependence of the interfacial structure on its orientation and temperature (here proportional to $-a_2$), based on computations for the same parameters as employed for the interphase boundaries, i.e., $a_3 = -12$, $a_{42} = 1$, as well as appropriate asymptotic analysis of the governing equations.

5.1.1. The isotropic case and special $\hat{n}$ that lie in the $(1\bar{1}0)$ mirror plane

For $\epsilon^2 = B/A = 1$, we have $\xi_x = \xi_y = \xi_z = 1$, and the interface orientation drops out of the problem. Symmetry allows solutions with $X(\zeta) = Y(\zeta)$, and an isotropic surface tension results.

For general values of B/A, orientations [hhk] in the $(1\bar{1}0)$ mirror plane lead to $\xi_x^2 = \xi_y^2$, and solutions with $X(\zeta) = Y(\zeta)$ are possible in this case as well. For the [111] orientation, here is the further simplification that $\xi_x^2 = \xi_y^2 = \xi_z^2 = \xi^2 = (1 + 2\epsilon^2)/3$. In this case the governing equations then simplify to the form

$$2\xi^2 X_{\zeta\zeta} = h_X(X, Z), \tag{90a}$$

$$\xi^2 Z_{\zeta\zeta} = h_Z(X, Z), \tag{90b}$$

where $h(X, Z) \equiv f(X, X, Z)$ represents the free energy density and $\xi^2 = (1 + 2\epsilon^2)/3$. For the purposes of finding analytical solutions, we used the semi-infinite domain $[0, \infty)$ with the appropriate symmetry conditions at the origin. When computing numerical solutions, we used a truncated domain that was sufficiently large that the solution did not change.

We conducted a series of computations for the [111] APB with a_2 varying in the range $0 < a_2 < a_2^c = 2$. Another type of wetting behavior is observed, as shown in Fig. 13, where the

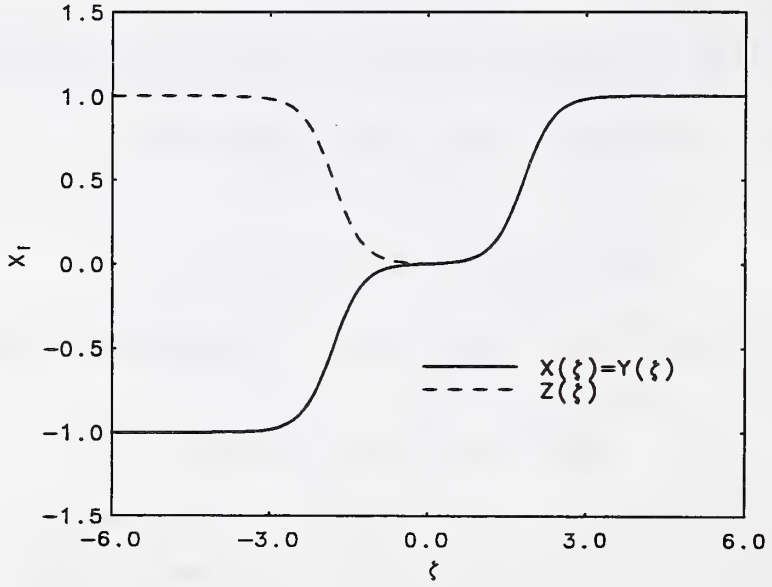

Figure 13: The [111] APB for $a_2 = 1.99999$, $a_3 = -12$, $a_{42} = 1$ and $\epsilon^2 = 0.005$.

order parameters though the antiphase boundary are plotted for $a_2 = 1.99999$. In this case the disordered phase intervenes between the two Cu_3Au variants on either side of the transition layer. As a_2 approaches a_2^c, the disordered region in the interior of the layer is found to widen at a logarithmic rate as $a_2 \to a_2^c$; an asymptotic analysis in this limit is presented in Section 5.1.3. In

contrast to the wetting behavior found for the [100] IPB, in which the wetting by $L1_0$ occurs for $\epsilon^2 \ll 1$ and $a_2 = a_2^c$, the wetting of the [111] APB by the disordered phase occurs as $a_2 \to a_2^c$ and is insensitive to the value of ϵ.

5.1.2. The general orientations including the [100] APB

In contrast to the [100] IPB considered above, the imposed boundary conditions Eq. (87) and Eq. (88) for the [100] APB do not allow the symmetry $Y(\zeta) = Z(\zeta)$, but instead allow solutions in which $X(\zeta)$ and $Y(\zeta)$ are odd and $Z(\zeta)$ is even. The governing equations (32) may then be solved on the semi-infinite interval, $[0, \infty)$, with the boundary conditions

$$X(0) = Y(0) = 0, Z'(0) = 0, \text{ and } X(\zeta) = Y(\zeta) = Z(\zeta) = \chi_1 \text{ as } \zeta \to \infty. \tag{91}$$

Numerical solutions of the governing equations for the [100] APB with these boundary conditions for different values of ϵ and a_2 show somewhat more complicated interfacial structures than that found for the [100] IPB or the [111] APB: depending on the values of ϵ and a_2, the [100] APB can show the formation of an intervening layer composed of either $L1_0$ or disordered phase, or, in intermediate cases, combinations of the two, as described below.

For fixed values of $\epsilon^2 \sim 1$, an intermediate disordered layer is found to form as $a_2 \to a_2^c$, as illustrated in Fig. 14 for $a_2 = 1.99999$ and $\epsilon^2 = 0.25$. This behavior is similar to that found for the [111] APB in this limit.

On the other hand, as $\epsilon^2 \to 0$ for fixed values of $a_2 \neq a_2^c$, an intervening $L1_0$ layer is observed, that is analogous to the [100] IPB layering by $L1_0$. This is illustrated in Fig. 15 for $a_2 = 1.9$ and $\epsilon^2 = 0.005$. For this case the occupation densities are also shown Fig. 16. They may be compared with the APB results of Kikuchi and Cahn (1979, their Fig. 11(a)); again the similarity is striking. Similar results have been obtained by the improved cluster variation calculations of Finel *et al.* (1990).

In Fig. 17 we display the solution for $a_2 = 1.99999$ and $\epsilon^2 = 0.005$. Comparing Fig. 14 and Fig. 17, which both display solutions for $a_2 = 1.99999$ but different values of ϵ, we observe that the effect of reducing ϵ is to sharpen the transition between the interior region and the outer regions, but not to significantly alter the extent of the interior region. Comparing Fig. 15 and Fig. 17, which both display solutions for $\epsilon = 0.005$ but with different values of a_2, illustrates the widening of the

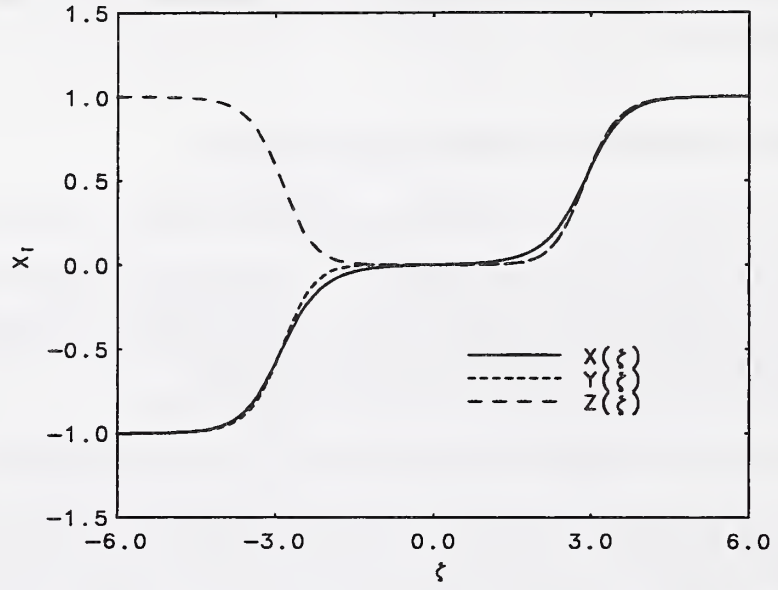

Figure 14: The [100] APB for $a_2 = 1.99999$, $a_3 = -12$, $a_{42} = 1$ and $\epsilon^2 = 0.25$.

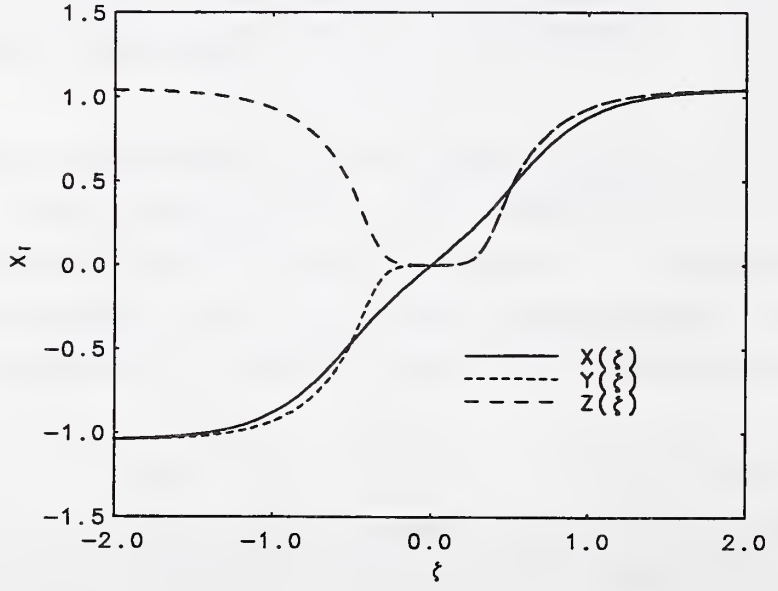

Figure 15: The [100] APB for $a_2 = 1.9$, $a_3 = -12$, $a_{42} = 1$ and $\epsilon^2 = 0.005$.

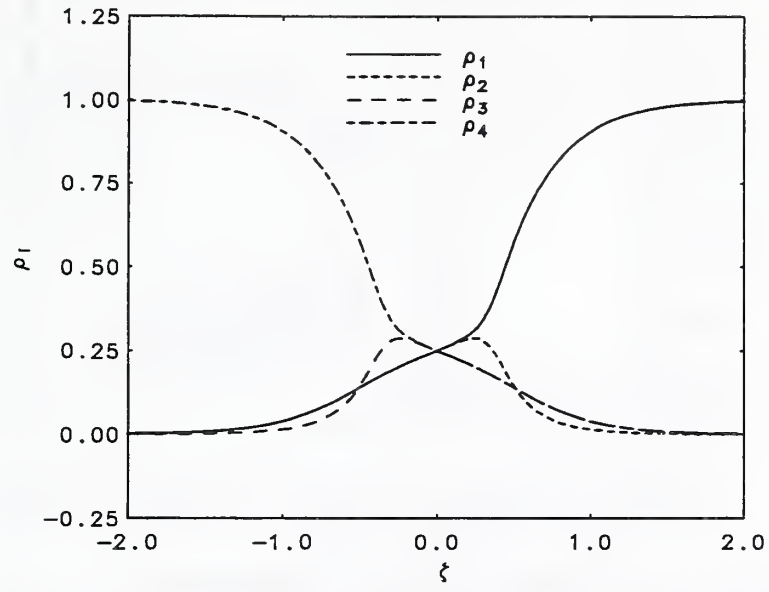

Figure 16: The occupation densities in the [100] APB for $a_2 = 1.9$, $a_3 = -12$, $a_{42} = 1$ and $\epsilon^2 = 0.005$. Once again the comparison with the results of Kikuchi and Cahn (1979, their Figure 11a) is striking.

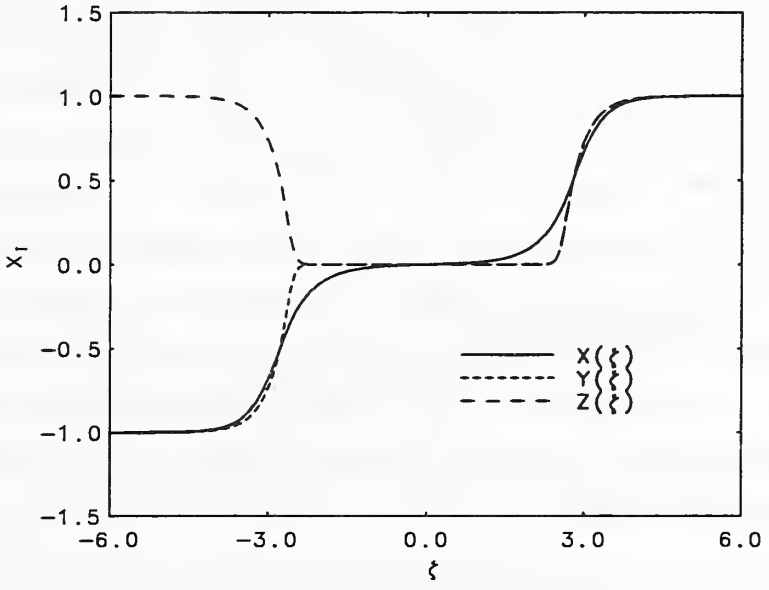

Figure 17: The [100] APB for $a_2 = 1.99999$, $a_3 = -12$, $a_{42} = 1$ and $\epsilon^2 = 0.005$.

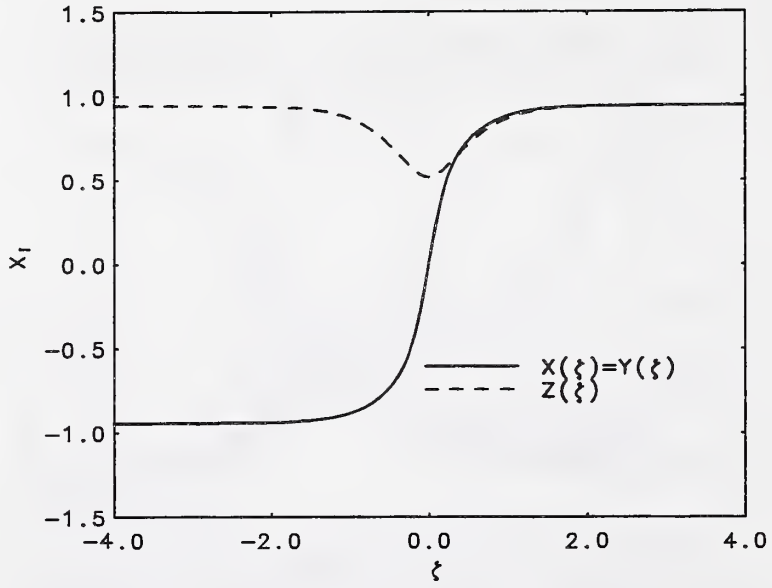

Figure 18: The order parameter variation in the [001] APB for $a_2 = 2.1$, $a_3 = -12$, $a_{42} = 1$ and $\epsilon^2 = 0.05$. Note that this APB separates metastable ordered variants ($a_2 > a_2^c$); the APB is practically the same for $a_2 < a_2^c$.

interior region as $a_2 \to a_2^c$. In the light of these observations we discuss in Section 5.1.4 below an asymptotic analysis as $\epsilon \to 0$.

Computed [001] APBs are shown in Fig. 18 through Fig. 20. These antiphase boundaries do not wet with the disordered phase in the limit $a_2 \to a_2^c$; in fact, other than the change in the far-field values $\pm\chi_1$, the solution behavior is insensitive to the value of a_2 provided it is not too close to a_2^L. The order parameters for $\epsilon^2 = 0.05$ and $a_2 = 2.1$ are shown in Fig. 18; the corresponding occupation densities are shown in Fig. 19. These solutions show that it is possible to compute antiphase boundaries between metastable $L1_2$ phases; for these values of the parameters the disordered phase is the lowest energy bulk state. Fig. 20 shows the order parameters for $\epsilon^2 = 0.005$ and $a_2 = 2.1$, showing that there is a significant dependence on ϵ in these solutions. This strong dependence suggests that another asymptotic analysis may be carried out as $\epsilon \to 0$; we report those results in Section 5.1.5.

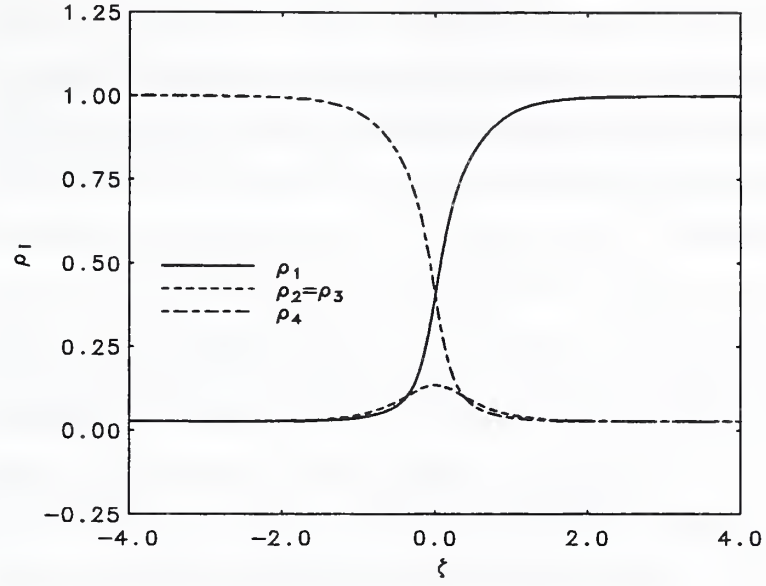

Figure 19: The occupation density variation in the [001] antiphase boundary for $a_2 = 2.1$, $a_3 = -12$, $a_{42} = 1$ and $\epsilon^2 = 0.05$.

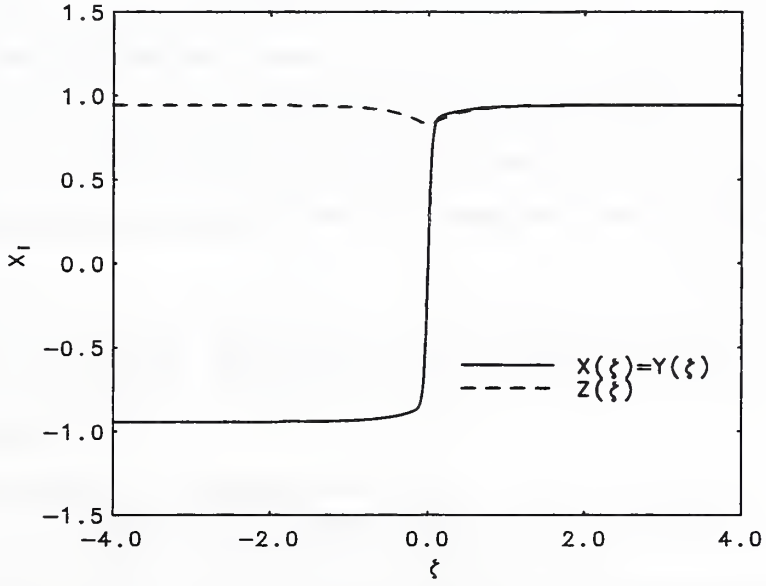

Figure 20: The order parameter variation in the [001] APB for $a_2 = 2.1$, $a_3 = -12$, $a_{42} = 1$ and $\epsilon^2 = 0.005$.

5.1.3. The asymptotic limit $a_2 \to a_2^c$ for the [111] APB

We define $\delta = a_2^c - a_2$ and consider Eq. (90) in the limit $\delta \to 0$. From Eq. (89) we find that $\chi_1 = 1 + \delta/a_2^c + \mathcal{O}(\delta^2)$ as $\delta \to 0$, and so the energy density in the bulk phases is $h(\chi_1, \chi_1) = -3\delta + \mathcal{O}(\delta^2)$ as $\delta \to 0$. The governing equations may be integrated once; on applying the expression for the free energy in the bulk phase, this gives

$$\xi^2 \left[X_\zeta^2 + \frac{Z_\zeta^2}{2} \right] - h(X, Z) = 3\delta + \mathcal{O}(\delta^2). \tag{92}$$

We anticipate the formation of an interior region occupied by disordered material, i.e., where $X(\zeta)$ and $Z(\zeta)$ and their first derivatives are small. In the interior region the leading order terms in the first integral, Eq. (92), are $\mathcal{O}(\delta)$ and it is a simple matter to show that this requires $X(\zeta)$ and $Z(\zeta)$ to be $\mathcal{O}(\delta^{1/2})$. In the disordered region, we express the solution as $X(\zeta) = \delta^{1/2}[\bar{X}^{(0)}(\zeta) + \mathcal{O}(\delta)]$ and $Z(\zeta) = \delta^{1/2}[\bar{Z}^{(0)}(\zeta) + \mathcal{O}(\delta)]$. The leading-order solutions are then found to be

$$\bar{X}^{(0)}(\zeta) = A^{(0)} \sinh\left(\frac{\sqrt{2a_2^c}}{\xi} \zeta \right), \tag{93}$$

and

$$\bar{Z}^{(0)}(\zeta) = B^{(0)} \cosh\left(\frac{\sqrt{2a_2^c}}{\xi} \zeta \right), \tag{94}$$

where $A^{(0)}$ and $B^{(0)}$ are constants, and we have chosen to centre the interface at $\zeta = 0$.

The disordered region separates two outer regions where $X(\zeta)$ and $Z(\zeta)$ are not small; we denote the outer region for $X > 0$ as region I, and the outer region for $X < 0$ as region II. The solutions $X(\zeta)$ and $Z(\zeta)$ in these outer regions are given by regular perturbation series in δ. The leading-order solutions are

$$X^{(0)}(\zeta) = Z^{(0)}(\zeta) = \frac{1}{2}\left[1 + \tanh\left(\frac{\zeta}{\xi}\sqrt{\frac{a_2^c}{2}} - \ell(\delta) \right) \right], \tag{95a}$$

in region I, and

$$-X^{(0)}(\zeta) = Z^{(0)}(\zeta) = \frac{1}{2}\left[1 - \tanh\left(\frac{\zeta}{\xi}\sqrt{\frac{a_2^c}{2}} + \ell(\delta) \right) \right], \tag{95b}$$

in region II. Here $\ell(\delta)$ is a function of δ to be determined, and we assume that $\ell(\delta) \to \infty$ as $\delta \to 0$.

Matching the outer regions to the interior region gives that $A^{(0)} = B^{(0)}$. Substituting the form for the inner region in the first integral, Eq. (92), evaluated at $\zeta = 0$ gives that $A^{(0)} = B^{(0)} = \sqrt{3/a_2^c}$.

Matching also requires that

$$\ell(\delta) = -\left[\frac{\ln\delta + \ln(3/4a_2^c)}{4}\right]. \tag{96}$$

The asymptotic solution compares favourably to the numerical solutions; the error in the layer width (based on $Z(\zeta^*) = 0.5$ in this case) is $O(\delta)$ for sufficiently small δ. Eq. (96) predicts that the length of the interior disordered region $\ell(\delta)$ increases logarithmically as $\delta \to 0$, i.e., as $a_2 \to a_2^c$. We also note that the two outer solutions, given by Eq. (95), closely approximate a pair of IPBs symmetrically displaced from the centre of the interface. This suggests that the ABP may be thought of comprising two IPBs which separate as $a_2 \to a_2^c$, as has been suggested by Kikuchi and Cahn (1979) and by Widom (1978), and discussed more recently by Finel *et al.* (1990).

5.1.4. The asymptotic limit $a_2 \to a_2^c$, $\epsilon \to 0$ for the [100] APB

We first take the limit $\epsilon \to 0$ and find that like the [100] IPB, there are three regions on the interval $[0, \infty)$. There are two outer regions where the solutions are given by regular perturbation series in ϵ. In both outer regions the leading-order solution for $X(\zeta)$ satisfies

$$X^{(0)}_{\zeta\zeta} = 2a_2X^{(0)} + a_3(Z^{(0)})^2 + 4[(X^{(0)})^2 + a_{42}(Z^{(0)})^2]X^{(0)}. \tag{97}$$

Outer region I (where $\zeta < \zeta^*$) has at leading order $Z^{(0)}(\zeta) \equiv 0$, where ζ^* is at this stage undetermined. Outer region II (where $\zeta > \zeta^*$) has

$$Z^{(0)}(\zeta) = \pm\sqrt{-\frac{2a_2 + a_3X^{(0)}(\zeta) + 2a_{42}(X^{(0)}(\zeta))^2}{2[2 + a_{42}]}}. \tag{98}$$

The inner region, centred at $\zeta = \zeta^*$ with width $\epsilon^{2/3}$, follows very closely the case of the interphase boundary.

Matching across the inner region shows that the leading-order outer solutions are continuous. As a result, in both outer regions, $X^{(0)}(\zeta^*) = X^c$, where X_c is given by the value $X^{(0)}$ for which $Z^{(0)} = 0$ in outer region II.

There is a first integral of the governing equations

$$\frac{X_\zeta^2}{2} + \epsilon^2 Z_\zeta^2 - f(X, Z, Z) = -f(\chi_1, \chi_1, \chi_1). \tag{99}$$

In outer region I, $Z^{(0)} = 0$ and so we may integrate once more to find

$$\zeta^* = \sqrt{2}\int_0^{X_c} \frac{d\nu}{\sqrt{f(\nu, 0, 0) - f(\chi_1, \chi_1, \chi_1)}}. \tag{100}$$

We may examine how the length of the outer region I, given by $\zeta^\star$, varies as a_2 approaches a_2^c, by taking the limit $\delta \to 0$, where $\delta = a_2^c - a_2$. As shown in the case of the [111] APB, $f(\chi_1, \chi_1, \chi_1) = -3\delta + \mathcal{O}(\delta^2)$, and so Eq. (100) becomes

$$\zeta^\star = \sqrt{2} \int_0^{X_c} \frac{d\nu}{\sqrt{\nu^4 + a_2^c \nu^2 + 3\delta + \mathcal{O}(\delta^2)}}. \tag{101}$$

In the limit $\delta \to 0$, we find

$$\zeta^\star = \sqrt{\frac{2}{a_2^c}} \sinh^{-1}\left(X_c \sqrt{\frac{a_2^c}{3\delta}} \right) + \mathcal{O}(\delta), \tag{102}$$

and so

$$\zeta^\star = -\frac{1}{\sqrt{2a_2^c}} \ln(\delta) + \mathcal{O}(1), \; \delta \to 0. \tag{103}$$

Thus the width of outer region I increases logarithmically as a_2 approaches a_2^c much like the width of the disordered region for the [111] APB.

We have compared our asymptotic analysis to our numerical solutions. In Fig. 21, we compare

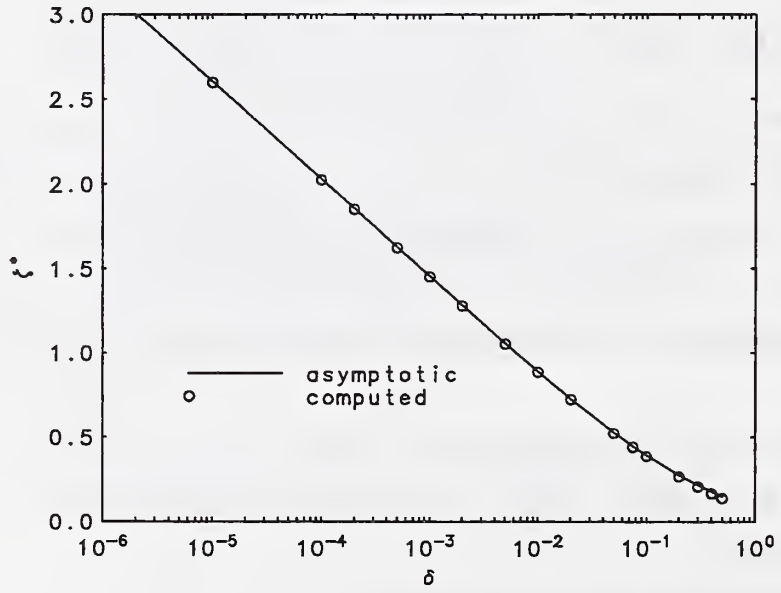

Figure 21: Comparison of asymptotic (solid line) and numerically computed values (circles) of $\zeta^\star$ against δ.

the asymptotic form for $\zeta^\star$ predicted by our asymptotic analysis, Eq. (102), with that determined from our numerical solutions. There is evidently excellent agreement; for $\epsilon^2 = 0.005$ and $\delta = 10^{-4}$,

the relative error in the asymptotic solution for the layer width compared to the computed value of $\zeta^* \approx 2.5978$ is about 0.26%.

This analysis suggests that for small ϵ, as a_2 approaches a_2^c, the APB is composed of two IPBs symmetrically displaced from the centre of the interface, both of which exhibit wetting by the $L1_0$ bulk phase, this is most clearly evident in Fig. 17. Such behavior was also suggested by Kikuchi and Cahn (1979); our Fig. 17 shows excellent agreement with Fig. 6 of Finel *et al.* (1990).

5.1.5. The asymptotic limit $\epsilon \to 0$ for the [001] APB

Fig. 18 and Fig. 20 show the structure of the order parameters for the [001] APB. As ϵ decreases, the magnitude of the dip in the Z profile diminishes at a rate proportional to ϵ, and the X profile appears to approach a tanh function of width ϵ. That behavior motivates our matched asymptotic analysis for this case. It is sufficient to consider the domain $\zeta \geq 0$ with the boundary conditions $X(0) = Z_\zeta(0) = 0$ and $X, Z \to \chi_1$ as $\zeta \to \infty$. In this case $X(\zeta) = Y(\zeta)$ because the boundary conditions do not break the symmetry of the governing equations, and it is sufficient to consider the domain $\zeta \geq 0$ with the boundary conditions $X(0) = Z_\zeta(0) = 0$ and $X, Z \to \chi_1$ as $\zeta \to \infty$.

We define an inner variable $\zeta = \rho\epsilon$, and expand the dependent variables as

$$X = x_0(\rho) + \epsilon x_1(\rho) + \ldots \text{ and } Z = \chi_1 + \epsilon z_1(\rho) + \ldots . \tag{104}$$

At the first non-trivial order, we find that

$$x_0 = \chi_1 \tanh\eta, \text{ and } z_1 = C_1 + C_2\rho, \tag{105}$$

where $\eta = \alpha\rho$ and $\alpha = \sqrt{3}\chi_1$. We require $z_1'(0) = 0$, so $C_2 = 0$. At next order, we find that, after satisfying the boundary conditions,

$$z_2 = -\frac{4\chi_1 - 12}{3} \ln \cosh\eta + C_3 \tag{106}$$

and

$$x_1 = \frac{-C_1\chi_1(4\chi_1 - 12)}{64\alpha^2} \mathrm{sech}^4\eta \left[8\eta + 8\eta\cosh 2\eta + 4\sinh 2\eta + 2\sinh 4\eta\right]. \tag{107}$$

We seek outer solutions of the form

$$X = \chi_1 + \epsilon X_1(\zeta) + \ldots \text{ and } Z = \chi_1 + \epsilon Z_1(\zeta) + \ldots . \tag{108}$$

We find that

$$Z_1 = \left(\frac{3\chi_1}{3-\chi_1}\right) X_1 = C_1 e^{-\lambda\zeta}, \tag{109}$$

$$Z_2 = C_4 e^{-\lambda\zeta} + C_1^2 f_1(\chi_1) e^{-2\lambda\zeta}, \tag{110}$$

for $\lambda > 0$ given by

$$\lambda^2 = (16/3)\chi_1^2 + 28\chi_1 - 24 \tag{111}$$

and

$$f_1(\chi_1) = \frac{1}{3\lambda^2}\left[\frac{(4\chi_1 - 12)(3-\chi_1)}{3\chi_1} + 18 - 4\chi_1\right]. \tag{112}$$

Matching the inner and outer solutions yields $C_1 = \alpha(4\chi_1 - 12)/(3\lambda)$, which completes the solution through $O(\epsilon)$. The comparison between asymptotic and numerical solutions for $Z(0)$ with $\epsilon \ll 1$ is excellent.

For $\epsilon \ll 1$ the surface energy of the [001] APB is found to be relatively small compared to the [100] and [110] APBs; this behavior is consistent with the geodesic interpretation of the [001] surface energy, which takes the form

$$\gamma = \int_{(-\chi_1,\chi_1)}^{(\chi_1,\chi_1)} \sqrt{2f(X,X,Z)}\sqrt{2\epsilon^2 X^2 + dZ^2} \tag{113}$$

where we have set $Y = X$. Since the Z-variation of the solution is small for $\epsilon \ll 1$ (c.f. Fig. 20), the geodesic curve tends to a line of constant Z in the (X, Z) plane. The weighted arclength dS is therefore small along the geodesic, resulting a low surface energy.

5.2. Interfacial energy

The orientation dependence of the interfacial energy of the APB solutions is illustrated in Fig. 22 and Fig. 23. The interfacial energy is now a function of two parameters, the "temperature" a_2 and the ratio of the gradient energy coefficients ϵ^2. We have computed the orientation dependence for a number of different cases; we will present a small subset of these results and defer more detailed results to a subsequent paper.

Because of the broken symmetry due to the $1 \leftrightarrow 4$ shift, the APB interfacial energy has $4/mmm$ tetragonal symmetry as shown in Fig. 22 and Fig. 23. The [001] APB has low energy (where the solution behaves as in Section 5.1.5), and the [100] and [110] APBs have high energies (see Section 5.1.4).

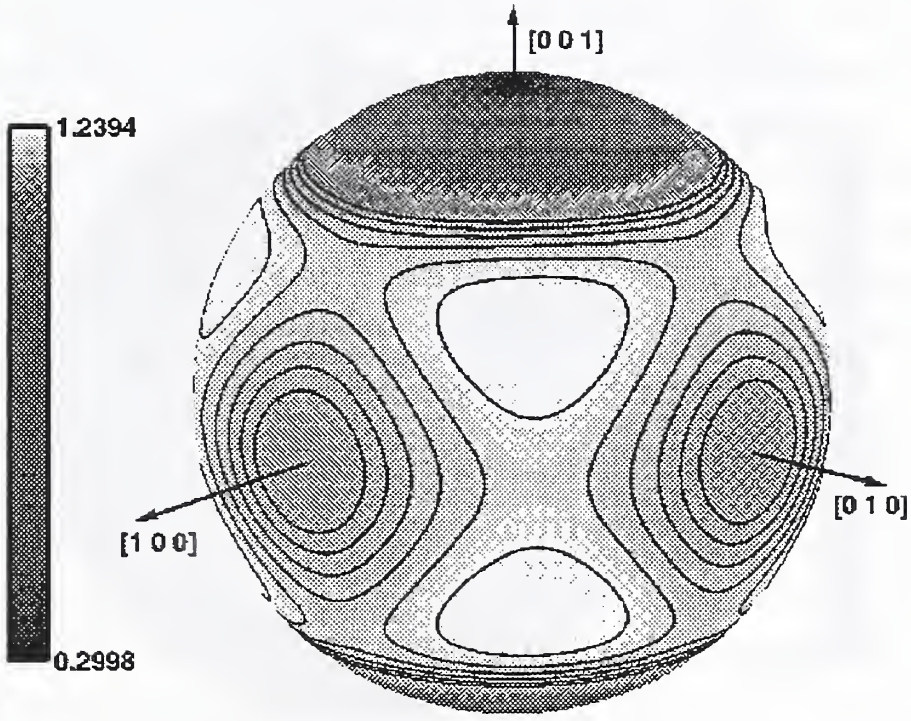

Figure 22: APB interfacial energy variation for $a_2 = 1.99$ and $\epsilon^2 = 0.005$.

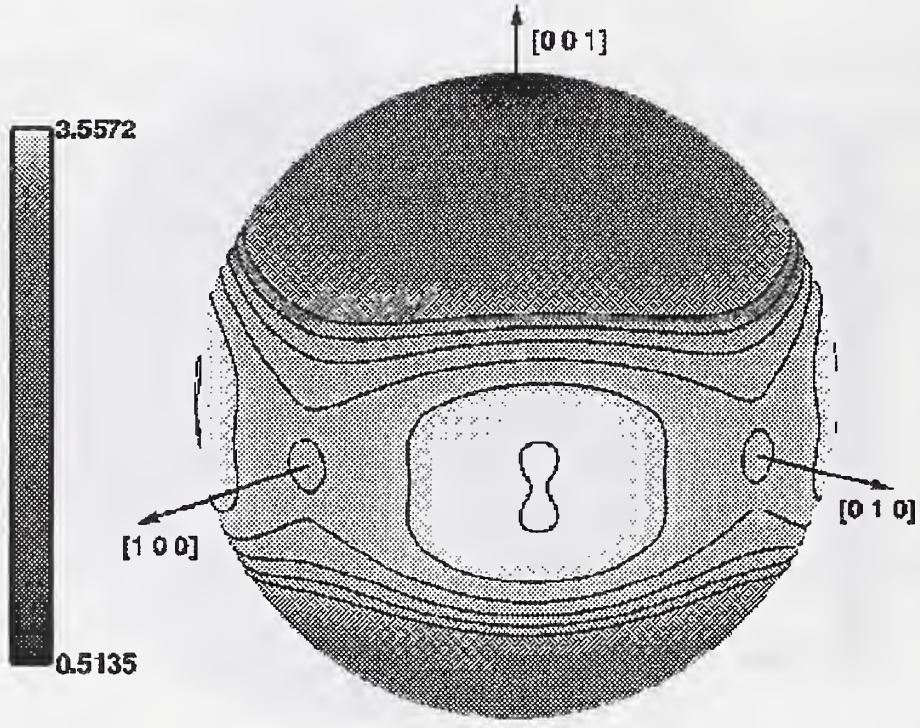

Figure 23: APB interfacial energy variation for $a_2 = 1.5$ and $\epsilon^2 = 0.005$.

Note that the location and number of extrema in the energy depend on the parameters. As a_2 approaches a_2^c, the maxima of the interfacial energy tend to the $< 111 >$ directions and the anisotropy diminishes. This behavior is consistent with the energy of the APB approaching the behavior of two separated IPB as a_2^c is approached (Kikuchi and Cahn 1979). As a_2 decreases from a_2^c, the maxima in the interfacial energy tends to the $< 110 >$ directions and the anisotropy becomes stronger. At some distinguished value of a_2, there is a bifurcation of the maxima at the $< 110 >$ directions into two maxima and saddle, while the saddles at $< 100 >$ become minima and two saddles each of which move toward [001] and $[00\bar{1}]$ along the $< h0k >$. Fig. 23 shows the energy for the case when a_2 is slightly larger than this critical value. More detailed investigation of this behavior will appear elsewhere.

In the CVM calculations of Kikuchi and Cahn (1979), the interfacial energy of some of the orientations vanished as the critical point was approached because they only took into account nearest-neighbor interactions in their tetrahedral approximation. Because our continuum formulation models both first and second nearest-neighbor interactions, our model has nonzero interfacial energy for all orientations.

The anisotropic interfacial energies were used to compute the ξ-vectors in the same manner as in Section 4, where the ξ-vector based on the IPB surface energy was used to compute the IPB equilibrium shape. We will refer to the analogous shape computed from the APB surface energy as a ξ-surface, and refer to the convex inner portion of the possibly non-convex ξ-surface as the Wulff shape. One octant from the resulting ξ surfaces are shown in Fig. 24 and Fig. 25. For $a_2 = 1.99$ and $\epsilon^2 = 0.005$ (Fig. 24) the anisotropy is strong enough to cause "ears" to form; this implies the the ξ-surfaces for these parameters have edges that are almost circular. The Wulff shapes correspond to the appropriately reflected ξ surface with the ears removed; in these cases the Wulff shape resembles a slightly bulging almost circular coin. Such Wulff shapes could be expected on the basis of the tetragonal symmetry caused by the different behaviours of the $1 \leftrightarrow 4$ interchange in the [001] direction *vs.* the [100] and [110] directions. Congruent rotated shapes are obtained for the other interchanges. The formation of the edges can be considered to develop parametrically with decreasing ϵ^2 for fixed a_2. For a given a_2, the edges may first appear at either $< 0kl >$ or $< hhl >$ directions for decreasing ϵ^2. The edges then widen over a very small range of ϵ^2 until a complete ear rings the ξ surface. This picture of domain structures composed of large flat segments of low energy

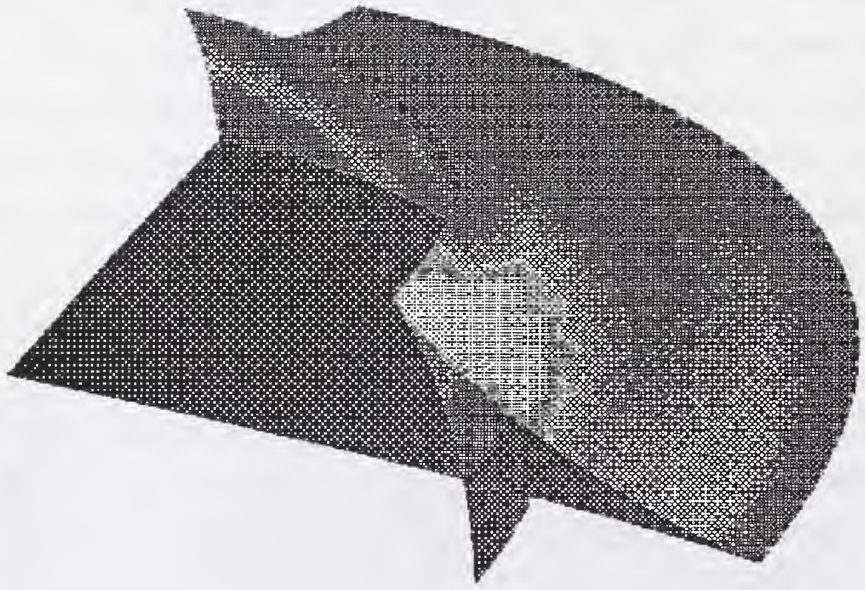

Figure 24: One-eighth of the ξ surface for $a_2 = 1.99$ and $\epsilon^2 = 0.005$.

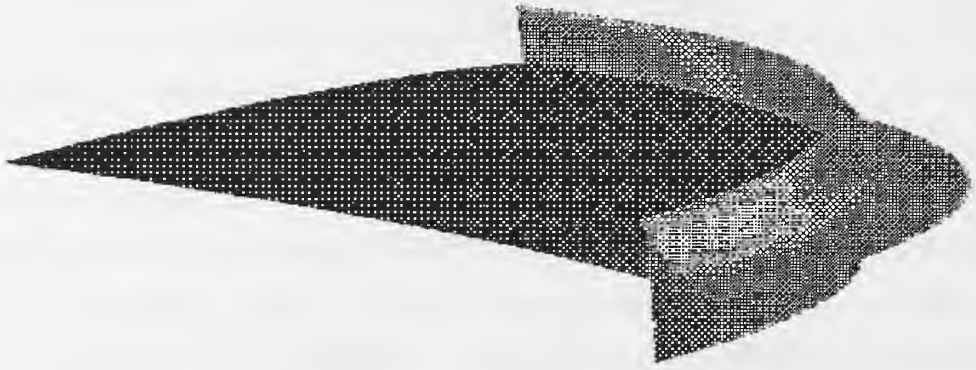

Figure 25: One-eighth of the ξ surface for $a_2 = 1.5$ and $\epsilon^2 = 0.005$.

surfaces in the three cube orientations together with sharp corners to smoothly curved segments is readily seen in the micrographs of the classic study of Fisher and Marcinkowski (1961). These shapes confirm the conclusion of Kikuchi and Cahn (1979). The competition of these faces in the three-dimensional ordering of an $L1_2$ alloy can now be computed using our model; we are currently studying this situation.

6. Other interfaces

There are additional phase boundaries in our model that could also be investigated. For example, as illustrated in Fig. 4, the model includes the possibility of stable bulk $L1_0$ phases, which have a total of six variants at a given temperature. Each variant is characterized by a single non-zero component X_0 of the order parameters, with the six variants $(\pm X_0, 0, 0)$, $(0, \pm X_0, 0)$, or $(0, 0, \pm X_0)$, and describes a bulk phase which is ordered in planar layers. Antiphase boundaries connecting any two of the variants can be examined, and the associated surface energy calculated. Two basic types of $L1_0$ APBs result, depending on whether the two variants: (i) are each described by the same component of the order parameters taking equal and opposite signs, say $(X_0, 0, 0)$ and $(-X_0, 0, 0)$ in each domain, or (ii) are described by different non-zero components, say $(X_0, 0, 0)$ and $(0, X_0, 0)$. The former case (i) has a simple analytical solution for any orientation, given by a hyperbolic tangent profile, from which the orientation dependence of the surface energy can be obtained in closed form, and the surface energy is given by

$$\gamma(\hat{\mathbf{n}}) = \frac{2}{3}|a_2|^{3/2}\sqrt{n_x^2 + \epsilon^2(n_y^2 + n_z^2)}; \tag{114}$$

in particular, the surface energy has tetragonal symmetry about the [100] direction. We note that this closed form solution makes the energy stationary, but does not necessarily correspond to the global energy minimum, which, for example, could entail contributions from additional order parameters.

In the latter case (ii), the planar layers in each domain are mutually perpendicular and, as there is generally a mismatch in the lattice parameters at an APB of this type, elastic effects can become important. The resulting surface energy does not have a closed form solution, but symmetry arguments (Kalonji and Cahn 1982) show that the resulting surface energy again has tetragonal symmetry, with the tetragonal axis perpendicular to the normals to each family of layers.

IPB energies can be computed for all pairs of phases over the range of temperature or composition of coexistence. Kikuchi and Cahn (1979) computed the IPB between fcc and $L1_2$ over a range of temperatures to the triple point allowing W to vary, and showed an infinite temperature coefficient of the energy at the congruent point and wetting by $L1_0$ at the triple point. Because of the fourth order truncation of the free energy and our decision to keep concentration constant we are limited to the kinds of coexistences the model gives, similar to those found by Nix and Shockley (1938). As seen in fig. 4, there is a range of a_2 where both $L1_2$ and $L1_0$ are stable, and for some range of parameters there is a point where they have equal free energy. For this case there is no coexistence between fcc and $L1_0$. Such coexistence is commonly seen in phases diagrams, but is absent from the phase diagram found by Nix and Shockley with such a free energy, and is also absent from Lifshitz' original predictions from the Landau theory.

7. Discussion

The model developed in this paper is an attempt to overcome the ad hoc approach employed by phase-field models to represent anisotropic interfaces. Here we have focussed on the case of an fcc lattice and have developed a model which is intimately related to the lattice and is formulated in terms of physically based order parameters. Our model employs an energy functional in which the gradient energy terms are simple square terms and results in a simple continuum description of an interface. This model provides a natural development of phase-field models. By conducting both asymptotic analysis and numerical solutions of the resulting system of nonlinear ordinary differential equations that represent stationary interfaces we have been able to analyse many interesting features of both IPBs and APBs, and have exhibited phenomena that have only previously been observed in much more complicated numerical simulations. We anticipate that the approach adopted here can be adapted to other crystalline structures.

One way to incorporate anisotropic interfacial properties in a single-order-parameter diffuse interface theory is to allow the gradient energy coefficient and the mobility coefficient τ (cf. Eq. (32)) to depend on the spatial gradient of the order parameter; in this way the surface energy σ and the kinetic coefficient μ can be assigned a given anisotropy. While this approach allows a great deal of flexibility, it is also somewhat *ad hoc*. Another approach to introducing anisotropy is through generalized gradient energy terms that include higher-order derivatives; this approach can also be

difficult to justify on theoretical grounds. The use of lattice models, or continuum models based on an underlying lattice such as we have have considered here, have the advantage that the anisotropy is introduced in a natural way, and correctly incorporates the crystal symmetries that are present.

7.1. IPBs

Based on the theory developed here, we have computed IPBs for interfaces between the disordered FCC and $L1_2$ states at the congruent point, or the $W = 1/4$ point on the T_0 curve. In the [100] IPB, our simplified model of the alloy recovers the intervening layering reminiscent of the $L1_0$ phase, even though the $L1_0$ phase does not exist as a bulk phase under the imposed conditions. This layering was first seen by Kikuchi and Cahn (1979) in their discrete model using CVM. It is somewhat surprising that the continuum model that we employ seems to reproduce their results so well; we view this as *post facto* support for the continuum theory. The behavior of the interface profiles in the order parameters allowed for an asymptotic analysis where we were able to compute the outer behavior and examine in detail the mathematical aspects of the layering. In particular, the presence of significant gradients of X in the layer allowed the existence of the layered solutions even when this state is not allowed as a uniform bulk phase.

Similar layering in interfaces between phases has been observed in the molecular dynamics computations by Landman *et al.* (1980,1981) and Cleveland *et al.* (1982). They carried out surface molecular dynamics calculations for crystal growth in liquid phase epitaxy; their calculation included a bulk liquid part and surface part of 500 particles each. They found, among some transient phenomena, a persistent ordering within the interfacial layer. Their intralayer ordering is based on occupying a lattice, and not based on different occupation of two species on the lattice as is the case in our model. In any event, the layering in the interface that we observe is reminiscent of the intralayer ordering observed in their molecular dynamics calculations.

For a [100] IPB, the variational principle for the stationary interface's surface free energy can be written as

$$\gamma = \min_{X,Y,Z} \int_{-\infty}^{\infty} \left\{ \frac{1}{2} X_\zeta^2 + \frac{\epsilon^2}{2} Y_\zeta^2 + \frac{\epsilon^2}{2} Z_\zeta^2 + f(X,Y,Z) \right\} d\zeta, \tag{115}$$

with $(X,Y,Z) \to (0,0,0)$ as $\zeta \to -\infty$, and $(X,Y,Z) \to (1,1,1)$ as $\zeta \to +\infty$. The minimization with $Y = Z$ gives Eq. (65). For $\epsilon \ll 1$ this produces a transition from disordered phase to $L1_2$ phase with an intervening $L1_0$ layer ($Y = Z \approx 0$). Compare this behaviour to a *constrained* system

with no $L1_0$ layer, that is obtained by imposing $X = Y = Z$ in the variational principle Eq. (60); from Eq. (115) we have

$$\gamma(\mathrm{Cu_3Au}) = \min_X \int_{-\infty}^{\infty} \left\{ \frac{(A+2B)}{2} X_\zeta^2 + f(X,X,X) \right\} d\zeta, \tag{116}$$

giving now

$$(1+2\epsilon^2) X_{\zeta\zeta} = \frac{d}{dX} f(X,X,X) \tag{117}$$

This has a closed form solution with

$$\gamma(\mathrm{Cu_3Au}) = \frac{\sqrt{A+2B}\sqrt{a_{41}+a_{42}}}{\sqrt{6}}, \tag{118}$$

which exceeds the unconstrained minimum γ. The layering by $L1_0$ in the [100] IPB thus lowers the interfacial free energy of the boundary. Since the intervening $L1_0$ structure does not exist as a bulk phase under the conditions shown in Fig. 3 that were used for our calculations, this behavior is analogous to the prewetting behavior observed in the theory of critical point wetting (Cahn 1977), and also resembles surface melting of a solid-vapor interface at temperatures below the melting point (see, e.g., Lowen 1994).

In the [110] orientation, $X = Y$ with Z different, and no such layering occurs in the interfacial region. While two sites on the lattice are occupied with equal probability, the remaining two differ, and so there is no $L1_0$ layering in this orientation. The profile again matches very well with the discrete model of Kikuchi and Cahn (1979). For the [111] IPB all of the order parameters are equal, and a closed-form solution results.

One of the strengths of our theory is that we can also explore IPBs for general orientations. We have shown some results along these lines. Let us begin with the [111] IPB where all the order parameters are equal; proceeding toward [100] on an arc lying in the surface of the unit sphere, we find that $Y = Z$ smoothly separates from X as shown in Figure 10. Within about 25° of [100], the profiles tend to develop $L1_0$ layering behavior provided ϵ^2 is sufficiently small.

Setting out from [111] but in the direction of [110], we find that $X = Y$ smoothly separates from Z and continues to approach the behavior of the [110] IPB smoothly. Setting out from [110] toward [100] along the unit-radius arc connecting them, we find that Y separates from X and migrates over to Z; for orientations within the triangle X, Y, and Z are separated, approaching the special behaviors as orientations approach the side of the triangle (Figure 11).

7.2. APBs

For $L1_2$ antiphase boundaries we again find very favorable comparison with the previous discrete results of Kikuchi and Cahn (1979). The structure of the antiphase boundaries is very dependent on their orientation and the temperature. For interfaces whose normals lie in the vicinity of $< hk0 >$ (the equatorial surface energies), the solution passes through the origin in (X, Y, Z)-space. As the temperature approaches the transition temperature the energy of the well at the origin approaches that of the ordered phases. As a consequence the solution remains in the vicinity of the (X, Y, Z)-origin for longer spatial distances; compare Fig. 14 and 16. This corresponds to the interface being wetted by the disordered phase which may be represented by two IPBs. As a consequence the APB surface energy inherits the low degree of surface energy anisotropy associated with the IPB; compare the equatorial regions of Figs. 12 and 22.

For temperatures away from the transition temperature the equatorial surface energies of the APB have changed even though the structure of the interface shows that the solution in (X, Y, Z)-space still goes through the origin. This can be seen by comparing Figs. 22 and 23.

For interfaces whose normals lie closer to the tetragonal axis the solution is qualitatively different and does not pass through the origin in (X, Y, Z)-space; see Fig. 18. This results in a very large anisotropy (factors of 4 and 7) associated with interfacial normals lying in longitudinal planes; see Figs 22 and 23. The surface energy is no longer convex. The corresponding Wulff shape is a slightly bulging round coin, see Figs. 24 and 25.

7.3. Concluding remarks

In conclusion, we reiterate some of the successes and failures of our model. We obtain good comparison with previous discrete models (Kikuchi and Cahn 1979) for the spatial variation of the occupation of the lattice for IPBs and APBs. Our model is able to easily calculate one-dimensional interfacial profiles for general orientation. This allows us to determine the parametric variation of the interfacial energy of both IPBs and APBs, and via the Cahn-Hoffman ξ-vector, to determine equilibrium shapes or ξ-surfaces. We find that our model successfully incorporates both the cubic anisotropy of the IPBs and the tetrahedral anisotropy of the APBs in fcc crystals.[1]

[1]We have computed surface energies based on one-dimensional solutions that correspond to stationary, if not minimal, surface energies. We have not examined the possibility that the actual minimum energy solutions have

Although we have described the model in terms of the ordering of a binary alloy, the resulting model can also be interpreted in terms of solidification if we associate the liquid phase of a pure material with the disordered state of the alloy (a "lattice gas" liquid), and identify the solid phase of the material with a particular ordered state of the lattice that undergoes a first-order transition in passing from the ordered to the disordered state. This description then provides an alternate description of phase change allowing the anisotropy of the interface to arise in a natural way from the underlying crystal.

Our approach has focussed on the role played by the three order parameters X, Y, and Z that appear in the fcc model in determining the anisotropy of interphase boundaries and antiphase boundaries. We have not examined the role played by the overall composition variable W, which we have taken to be constant. This might be expected to give useful results for the description of antiphase boundaries that separate equivalent bulk domains having the same composition. For interphase boundaries, however, requirements of thermodynamic equilibrium generally require distinct values of W in each phase. Before thermodynamic equilibrium is attained, however, our model might be appropriate to the early stages of order-disorder transitions in systems that are initially of uniform composition, when the time scales for compositional diffusion are long compared to the times scales required for ordering to take place. Extension of our model to include concentration variation and to compute interfacial properties at specific locations on the phase diagram is currently underway (Braun *et al.* 1995b). In particular, the determination of the equilibrium phase diagram would determine the coefficients of the bulk part of the free energy, and matching the measured surface energy from experiment would then determine the gradient energy coefficients. We are also studying the motion of APBs in an effort to understand the facetting into (001) and (hk0) faces in three dimensions.

Acknowledgements

The authors are grateful for helpful discussions with W.C. Carter, S.R. Coriell, K. Elder, M.E. Gurtin, R.V. Kohn, D.J. Muraki, B.T. Murray, R.F. Sekerka, and particularly with W.J. Boettinger. We also thank J. Hagedorn and H.E. Rushmeier for help with visualization of data. JWC and GBM

lateral variations along the interface, and are described by two or three-dimensional solutions [see, for example, Morgan (1995)].

were partially supported by the Applied and Computational Mathematics Program of ARPA. AAW and GBM were partially supported by a NATO collaborative research grant.

References

[1] Allen, S. M., and Cahn, J. W. 1979 A microscopic theory for antiphase boundary motion and its application to antiphase domain coarsening. *Acta metall. mater.* **27**, pp. 1085–1095.

[2] Ansara, L., Sundman, B., and Wilemin, P. 1988 Thermodynamic modeling of ordered phases in the Ni-Al system. *Acta metall. mater.* **36**, pp. 977–982.

[3] Bader, G. and Ascher, U. 1987 A New Basis Implementation for a Mixed Order Boundary Value ODE Solver. *SIAM J. Sci. Stat. Comput.* **8**, pp. 483–500.

[4] Braun, R. J., Cahn, J. W., McFadden, G. B., Rushmeier, H.E., and Wheeler, A. A. 1995a Anisotropic equilibrium and growth shapes in the ordering of an fcc alloy. (In preparation).

[5] Braun, R. J., Cahn, J. W., McFadden, G. B., and Wheeler, A. A. 1995b Unpublished research.

[6] Caginalp, G., and Xie, W. 1993 Phase-field and sharp-interface alloy models. *Phys. Rev.* E **48**, pp. 1897–1909.

[7] Cahn, J. W. 1961 On Spinodal Decomposition. *Acta Metall.* **9**, pp. 795–801.

[8] Cahn, J. W. 1971 Thermodynamics of Solidification. In ASM Seminar Series on *Solidification* pp. 23–58. Metals Park, Ohio.

[9] Cahn, J. W. 1977 Critical Point Wetting. *J. Chem. Phys.* **66**, pp. 3667–3672.

[10] Cahn, J. W. and Allen, S. M. 1977 A microscopic theory for domain wall motion and its experimental verification in Fe-Al alloy domain growth kinetics. *J. Phys. (Paris) Colloque C7*, pp. C7-51–C7-54.

[11] Cahn, J. W., and Hilliard, J. E. 1958 Free energy of a nonuniform system. I. Interfacial free energy. *J. Chem. Phys.* **28**, pp. 258–267.

[12] Cahn, J. W., and Hoffman, D. W. 1974 A vector thermodynamics for anisotropic surfaces II. Curved and facetted surfaces. *Acta Metall. Mater.* **22**, pp. 1205–1214.

[13] Cahn, J. W., and Kikuchi, R. 1985 Transition layer in a lattice-gas model of a solid-liquid interface. *Phys. Rev.* B **31**, pp. 4300–4304.

[14] Cahn, J. W., and Novick-Cohen, A. 1994 Evolution Equations for Phase Separation and Ordering in Binary Alloys. *J. Stat. Phys.* **76** pp. 877–909.

[15] Clapp, P. C., and Moss, S. C. 1966 Correlation Functions of Disordered Binary Alloys - I. *Phys. Rev.* **142**, 418 - 427; 1968 *ibid.* - *II, Phys. Rev.* **171**, 754 - 763.

[16] Cleveland, C. L., Landman, U., and Barnett, R. N. 1982 Molecular dynamics of a laser-annealing experiment. *Phys. Rev. Lett.* **49**, pp. 790–793.

[17] Coriell, S. R., and McFadden, G. B. 1993 Morphological Stability. In *Handbook of Crystal Growth* (ed. D. T. J. Hurle) pp. 785–857. Amsterdam: Elsevier-North Holland.

[18] De Giorgi, E. 1978 Convergence problems for functionals and operators, *Proceedings of the International Meeting on Recent Methods in Nonlinear Analysis* (ed. Pitagoria) Bologna.

[19] Dupin, N. 1995 Contribution à l'évaluation thermodynamique des alliages polyconstitués à base de nickel. Ph. D. Thesis, Laboratoire de Thermodynamique et de Physico-Chimie Métallurgiques de Grenoble, Institut National Polytechnique de Grenoble.

[20] Evans, R. 1979 The nature of the liquid-vapour interface and other topics in the statistical mechanics of non-uniform, classical fluids. *Adv. Phys.* **28**, pp. 143–200.

[21] Finel, A. 1992 Thermodynamical Properties of Antiphases in fcc Ordered Alloys. In *Ordering and Disordering in Alloys* (ed. A. Yavari) New York: Elsevier Applied Science.

[22] Finel, A., Mazauric, V., and Ducastelle, F. 1990 Theoretical Study of Antiphase Boundaries in fcc Alloys. *Phys. Rev. Lett.* **65** pp. 1016–1019.

[23] Fisher, R. M. and Marcinkowski, M. J. 1961 Direct observation of antiphase boundaries in the $AuCu_3$ superlattice, *Phil. Mag.* **6**, pp. 1385–1405.

[24] de Fontaine, D. 1994 Cluster approach to order-disorder transformations in alloys. *Solid State Phys.***47**, pp. 33-176.

[25] Frank, F. C. 1962 Geometrical thermodynamics of surfaces, Chapter 1, *Metal Surfaces*, American Society of Metals, pp. 1–15.

[26] Fried, E. and Gurtin, M. E. 1994 Dynamic solid-solid transitions with phase characterized by an order parameter. *Physica* D **72**, pp. 287–308.

[27] Glicksman, M. E., and Marsh, S. P. 1993 The Dendrite. In the *Handbook of Crystal Growth* (ed. D. T. J. Hurle), pp. 1077–1122. Amsterdam: North Holland.

[28] Harowell, P. R., and Oxtoby, D. W. 1987 On the interaction between order and a moving interface: Dynamical disordering and anisotropic growth rates. *J. Chem. Phys.* **86**, pp. 2932–2942.

[29] Herring, C. 1951 Some theorems on the free energies of crystal surfaces. *Phys. Rev.* **82** pp. 87–93.

[30] Hilliard, J. E. 1970 Spinodal Decomposition. In *Phase Transformations* (ed. H. I. Aaronson) Metals Park, Ohio: American Society of Metals.

[31] Hoffman, D. W., and Cahn, J. W. 1972 A vector thermodynamics for anisotropic surfaces I. Fundamentals and application to plane surface junctions. *Surface Science* **31**, pp. 368–388.

[32] Huang, K. 1963 *Statistical Mechanics*, pp. 332-336. New York: Wiley.

[33] Kalonji, G., and Cahn J. W. 1982 Symmetry constraints on the orientation dependence of interfacial properties: The group of the Wulff plot. *J. Phys. Coll. C6* **43**, pp. C6-25–C6-30.

[34] Kessler, D. A., Koplik, J., and Levine, H. 1988 Pattern selection in fingered growth phenomena. *Advances in Physics* **37**, pp. 255–339.

[35] Kikuchi, R. 1951 A theory of cooperative phenomena. *Phys. Rev.* **81**, pp. 988–1003.

[36] Kikuchi, R., and Cahn, J. W. 1962 Theory of domain walls in ordered structures–II Pair approximation for nonzero temperatures. *J. Phys. Chem. Solids* **23**, pp. 137–151.

[37] Kikuchi, R., and Cahn, J. W. 1979 Theory of interphase and antiphase boundaries in fcc alloys. *Acta Metall.* **27**, pp. 1337-1353.

[38] Kobayashi, R. 1993 Modeling and numerical simulations of dendritic crystal growth. *Physica* D **63**, pp. 410–423.

[39] Lai, Z.-W. 1990 Theory of ordering dynamics for Cu_3Au. *Phys. Rev.* B **41**, pp. 9239–9256.

[40] Landau, L. D. 1937 On the theory of phase transitions. Reprinted in *Men of Physics: L. D. Landau*, Vol. 2: Thermodynamics, Plasma Physics, and Quantum mechanics. (ed. D. ter Haar), pp. 61–84. London: Pergamon.

[41] Landau, L. D. and Lifshitz, L., 1980. Statistical Physics. 3rd ed., Part 1. Vol. 5 of *Course of Theoretical Physics*. New York: Pergamon.

[42] Landman, U., Cleveland, C. L., and Brown, C. S. 1980 On the dynamics of epitaxial phase transformations. In *Ordering in Two Dimensions* (ed. S. K. Sinha) pp. 335–338 Amsterdam: Elsevier-North Holland.

[43] Landman, U., Cleveland, C. L., Brown, C. S., and Barnett, R. N. 1981 On the dynamics of epitaxial phase transitions. In *Nonlinear Phenomena at Phase Transitions and Instabilities* (ed. T. Riste) pp. 379–389. New York: Plenum.

[44] Lee, Y.W. and Aaronson, H.I. 1980 Anisotropy of coherent interphase boundary energy. *Acta metall.* **28**, pp. 539–548.

[45] Löwen, H. 1994 Melting, freezing, and colloidal suspensions. *Phys. Rep.* **237**, pp. 249–324.

[46] McFadden, G. B., Wheeler, A. A., Braun, R. J., Coriell, S. R., and Sekerka, R. F. 1993 Phase-field models for anisotropic interfaces. *Phys. Rev.* E **48**, pp. 2016–2024.

[47] Morgan, F. 1995 Lowersemicontinuity of energy of clusters, (preprint, Department of Mathematics, Williams College, Pennsylvania, USA)

[48] Moss, S. C. and Clapp, P. C. 1968 Correlation Functions of Disordered Binary Alloys - III *Phys. Rev.* **171**, 764–777.

[49] Murray, B. T., Boettinger, W. J., McFadden, G. B., and Wheeler, A. A. 1994 Computation of dendritic solidification using a phase-field model. In *Heat transfer in melting, solidification and*

crystal growth (ed. I. S. Habib and S. Thynell) pp. 67-76. New York: The American Society of Mechanical Engineers.

[50] Nicholas, J. F. 1968 Calculation of surface energy as a function of orientation for cubic crystals. *Aust. J. Phys.* **21**, pp. 21-34.

[51] Nix, F. C., and Shockley, W. 1938 Order-disorder transformations in alloys. *Rev. Mod. Phys.* **10**, pp. 1–71.

[52] Oxtoby, D. W. 1991 Crystallization of liquids: a density functional approach. In *Liquids, Freezing and Glass Transition* (ed. J. P. Hansen, D. Levesque, and J. Zinn-Justin), (Les Houches, Session LI, 1989) pp. 147–191. Amsterdam: Elsevier Science Publisher.

[53] Lord Rayleigh 1892 On the theory of surface forces.–II. Compressible fluids. *Phil. Mag.* **33**, pp. 209–220.

[54] Richards, M. J., and Cahn J. W. 1971 Pairwise interactions and the ground state of ordered binary alloys. *Acta metall.* **19**, pp. 1263–1277.

[55] Segel, L. A. 1965 The non-linear interaction of a finite number of disturbances to a layer of fluid heated from below. *J. Fluid Mech.* **21**, pp. 359–384.

[56] Shih, W. H., Wang, Z. Q., Zeng, X. C., and Stroud, D. 1987 Ginzburg-Landau theory for the solid-liquid interface of bcc elements. *Phys. Rev.* A **35**, pp. 2611–2618.

[57] Stanley, H. E. 1971 *Introduction to Phase Transitions and Critical Phenomena*, Oxford: Oxford University Press.

[58] Sternberg, P. 1991 Vector-valued local minimizers of nonconvex variational problems. *Rocky Mt. J. Math.* **21**, pp. 799-807.

[59] Taylor, J. E., and Cahn, J. W. 1994 Linking anisotropic sharp and diffuse surface motion laws via gradient flows, *J. Stat. Phys.* **77**, pp. 183-197.

[60] Voorhees, P. W., Coriell, S. R., McFadden, G. B., and Sekerka, R. F. 1984 The effect of anisotropic crystal-melt surface tension on grain boundary groove morphology. *J. Crystal Growth* **67**, pp. 425-440.

[61] van der Waals, J. D. 1893 Verhandel. Konink. Akad. Weten. Amsterdam (Sect. 1) **1**. For a translation, see Rowlinson, J. S. 1979 *J. Stat. Phys.* **20**, pp. 197–244.

[62] Warren, J. A. and Boettinger, W. J. 1995 Prediction of dendritic growth and microsegregation patterns in a binary alloy using the phase-field method. *Acta metall. mater.* **43**, pp. 689–703.

[63] Wheeler, A. A., Boettinger, W. J., and McFadden, G. B. 1992 Phase-field model for isothermal phase transitions in binary alloys. *Phys. Rev.* A **45**, pp. 7424–7439.

[64] Wheeler, A. A., Boettinger, W. J., and McFadden, G. B. 1993a Phase-field model of solute trapping during solidification. *Phys. Rev.* E **47**, pp. 1893–1909.

[65] Wheeler, A. A., and McFadden, G. B. 1995 A ξ-vector formulation of anisotropic phase-field models: 3-D asymptotics. *Euro. J. Appl. Math.*, in press.

[66] Wheeler, A. A., Murray, B. T., and Schaefer, R. J. 1993b Computation of dendrites using a phase field model. *Physica* D **66**, pp. 243–262.

[67] Widom, B. 1978 Structure of the $\alpha\gamma$ interface. *J. Chem. Phys.* **68**, pp. 3878–3883.